IEEE Access
Multidisciplinary ⋮ Rapid Review ⋮ Open Access Journal

Received 14 April 2024, accepted 9 May 2024, date of publication 20 May 2024, date of current version 24 May 2024.

Digital Object Identifier 10.1109/ACCESS.2024.3402686

APPLIED RESEARCH

Development of a Coaxial Dual-Coil Induction Heating System With a Composite Bridge-Type Inverter and a Flexible Switching Mechanism

TE-CHUN HUNG, (Member, IEEE), KUAN-CHIEH HUANG, (Member, IEEE), TSONG-SHING LEE, (Member, IEEE), JING-HONG LIN, CHEIEN-HUA CHEN, AND CHI-WEI LIAO

Department of Electrical Engineering, Southern Taiwan University of Science and Technology, Tainan 71005, Taiwan

Corresponding author: Kuan-Chieh Huang (kchuang07@stust.edu.tw)

ABSTRACT This study proposes a design of the composite bridge-type inverter with a flexible switching mechanism for a coaxial dual-coil induction heating system. Contemporary induction heating technologies predominantly adopt either a single-coil or multi-coil architecture. The former often suffers from limited heating coverage and lacks uniformity, while the latter is favored in applications necessitating broad heating ranges, requiring multiple inverters for effective coil switching control. Consequently, challenges persist in achieving rapid and consistent heating. In this regard, this study proposes a composite bridge-type inverter circuit comprising 5 power components. Through different power transistor switching mechanisms, the system enables independent or simultaneous operation of inner and outer coils, facilitating uniform and swift heating. Furthermore, the proposed inverter can adapt its coil architecture to various operating modes, optimizing heating consistency and performance. Notably, the system achieves an impressive efficiency rate of 96.2%. To validate the viability of our induction heating system concept, a laboratory prototype was constructed and tested. Results from the experiments affirm the system's flexible switching capabilities, catering to adjustable heating zone requirements in the coaxial dual-coil setup proposed in this study.

INDEX TERMS Composite bridge-type circuit, flexible switching mechanism, coaxial dual-coil induction heating system, uniform and swift heating.

I. INTRODUCTION

Induction heating technology operates on the principle of a heating coil induced with electricity to produce a magnetic field, which then generates eddy currents in the heating load to produce heat [1], [2]. It offers advantages such as fast heating speeds, high efficiency, and compliance with higher environmental and safety standards. This technology is applied in various industrial processes, medical settings, household stoves, and across different power levels [3], [4]. Particularly, induction heating technology is widely employed in household cooking appliances [5], [6]. Furthermore, in modern smart kitchens, cooking appliances are gradually transitioning to induction stoves from open-flame heating. Equipped with appropriate control mechanisms and communication systems, the realization of smart kitchens is achieved [7], [8].

At present, induction heating technology is used in household cooking stoves, and most of them come with a single heating coil and a single inverter [9]. Because this circuit

The associate editor coordinating the review of this manuscript and approving it for publication was Rui Li.

configuration has a low cost and reliable structure, it has become one of the top choices for the heating system of household cooking stoves. However, the heating range of the single-coil structure is limited, resulting in uneven heating [10], [11], [12]. Given this, to overcome the problem of uneven temperature in the heating load, coil layout architecture [6], [13], [14] and coil modular architecture [15], [16], [17] have been studied. However, these studies pertain to a wide range of heating applications with multiple heating loads. Under this framework, uniform heating for a fixed-point single load is barely achieved with a poor coil utilization rate, and this extra design does not lead to adding value to the heating system. In addition, the repeating coil is used for temperature compensation between the coil and the load [18]. While this may control load heating under a certain circumstance, however, the repeating coils change their main resonance characteristics when load misalignment presents, it cannot provide the energy to the load alone in general. Also, the loss caused by the continuous induction current of the repeating coil is not suitable for the fixed-point heating load. Moreover, a design using multi-coil architecture proposes to compensate for the heated load in a specific area, but there is still temperature unevenness when heating at a fixed point [19], [20], Furthermore, there are also some designs of induction heating systems for heating loads of different sizes and types [21], however, the problem of uneven heating of the load are barely addressed. None of the coil modularization, repeat coil technology, and multi-coil architecture designs mentioned above provide a better solution to the problem of uneven heating. The multi-coil architecture requires the same number of inverters and an involved control strategy to orchestrate the operation of inverters. This inevitably makes the overall heating system too large and complex, so the design of a multi-coil system is much more difficult compared with that of a single-coil system [22]. In general, heating circuits adopting a coaxial dual-coil structure [23] have a better temperature uniformity effect for fixed-point heating, due to the potent power supply that powers the inner and outer coil separately. However, impedances are different for the inner and outer coil, it also poses a very serious challenge due to the need to provide power supplies of different levels for the inner and outer coil. Reducing the number of inverters needed is one of the key points of discussion; some literature also improves the structure of inverters [24], [25], [26] to reduce the number of inverters and the overall circuit size, Additionally, some literature discusses the use of power components and the number of heating loads, paired with independent power control, utilizing different operating frequencies [12], [27], [28], [29], to achieve efficient electric power transmission. However, the control strategy for this type of circuit is quite complicated, and more rigorous consideration is required in the design process to avoid control errors that cause a heating system failure. Encouraging results of circuit design had gained from the aforementioned methods, but each of them may come with some demerits in certain respects, such as uneven heating in single-coil applications, the requirement of multiple inverters for multiple heating loads, and the complexity of control systems, there is still a lack of superior solutions to address these bottlenecks encountered in induction heating.

Therefore, this paper proposes a composite bridge-type inverter with a flexible switching mechanism for use in a coaxial dual-coil induction heating system to address the issue of uneven temperature rise in the heating load. By employing different control mechanisms for power transistors, the system enables the independent or simultaneous heating of the inner and outer coil, reducing the number of inverters required. This configuration allows for the adjustment of each coil's operational status based on heating requirements, optimizing heating uniformity and efficiency. The induction heating system compensates for temperature differences in the heating load area, enhancing speed and efficiency. Experimental verification through hardware prototyping confirms the system's temperature uniformity and rapid heating capabilities. The achievements, contributions, and technical features of this paper are listed as follows:

1) A composite bridge inverter is proposed, via switching control of power transistors, to achieve circuit structure change of the composite bridge.

2) The application of the coaxial dual-coil flexible switching mechanism helps to improve the heat distribution in the fixed-point heating application.

3) Integrating a composite bridge inverter and coaxial dual-loop coil reduces the number of inverters needed.

4) Applying the power transistor switching mechanism of the inverter provides flexible heating modes in response to different needs and heating occasions.

5) The coaxial dual-loop mutual inductance feature is used so that the unpowered coil can still perform energy repeat through induction. In addition to uniform heat distribution, it can also increase the heating speed.

The rest of this article is organized as follows. Section II introduces the proposed system, Section III discusses the parameter design and analysis of the resonant circuit, Section IV reports the experimental results, and Section V presents the conclusion.

II. SYSTEM ARCHITECTURE AND CONTROL STRATEGY

The dual-coil heating system using a composite bridge-type inverter proposed in this paper is shown in Figure 1. Figure 1(a) depicts a system circuit, including a composite bridge inverter circuit, a dual coil, a compensation circuit, and a feedback control system. The main power supply voltage V_{in} is the input of the composite bridge type inverter circuit, via turning on and off of the power transistors (Q_1, Q_2, Q_3, Q_4, and Q_5) in the inverter circuit, the DC voltage of the main power supply is converted into square wave voltage (v_m and v_t) which is applied to the dual-loop coil and its compensation circuit. When the square wave voltage (v_m and v_t) is applied on the coil and the compensation circuit, the induction heating coil (L_m and L_t) resonate in series with the compensation capacitors (C_m and C_t). Here C_m is the resonant capacitance

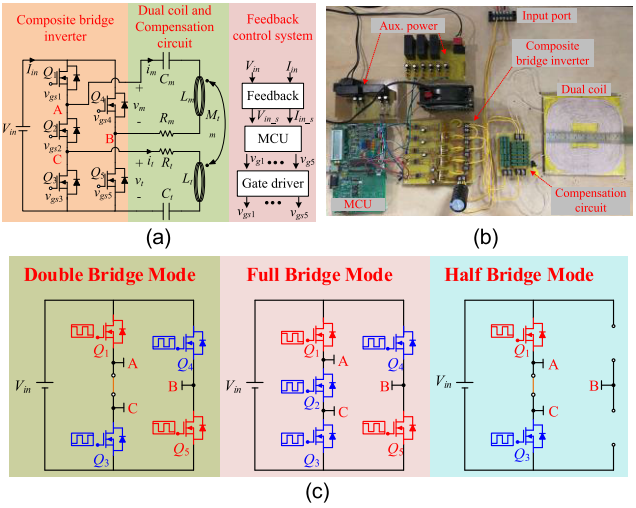

FIGURE 1. System schematic diagrams.

of the outer heating coil, L_m is the equivalent inductance of the outer coil, C_t is the resonant capacitance of the inner coil, and L_t is the equivalent inductance of the inner coil. The heating load is a stainless steel 304 iron plate, which will induce the magnetic field emitted by the coil and generate eddy currents for heating. R_t and R_m are the equivalent impedance of the heating load to the resonant tank of the inner coil and the outer coil, respectively, to simulate the load receiving the eddy current energy of the heating coil. Figure 1(b) is the photo of the actual circuit. Because the proposed composite bridge inverter circuit can change the operating status of the bridge circuit and the coil through the switching of the power transistors, next, the function and switching of each operation mode of the proposed architecture will be explained as shown in Figure 1(c). First, when the load needs to be heated up quickly, the induction heating system will operate in a dual-loop power supply mode. During this period, the left-side transistors of the inverter will be composed of Q_1 and Q_3, and the right-side transistors of the inverter will be composed of Q_4 and Q_5. The input power supply V_{in} applies DC voltage on the inverter circuit in this mode. Through the switching of the power transistors, the high-frequency square wave is applied to the resonant circuit consisting of the outer heating coil L_m and its compensation capacitance C_m, and the resonant circuit consisting of the inner heating coil L_t and its compensation capacitor C_t. Next, the energy is provided to both the inner and outer coils and their compensation capacitors, and both the inner and outer heating coils convert electricity into a magnetic field and transmit it to the load to complete the heating process. In this operation mode, the heating load temperature rising is faster because the circuit simultaneously supplies energy to both coils. When the load heats up until requiring a more uniform heat distribution, the system will switch to the outer-loop power supply mode. At this time, Q_1, Q_2, and Q_3 form the left-side transistors of the inverter, while Q_4 and Q_5 form the right-side transistors of the inverter. Through the switching of the power transistors, the input power V_{in} is converted into a high-frequency square wave and applied to the resonant circuit of the outer heating coil L_m and its compensation capacitor C_m. The energy of the resonant circuit is induced through the outer heating coil to the load to increase the heating on the outer coil area of the load. The energy of the outer coil will induce energy to the inner coil, which is also heat preservation of the central part of the load. In general, because of the smaller area of the central part of the heated load, the corresponding temperature rise is higher, while the temperature rise is lower for the outer part. Therefore, when the proposed inverter operates in this outer-loop power supply mode, it can concentrate the heating for the outer part of the load, and at the same time keep the central part warm through induction for a more uniform heat distribution. Finally, when the load needs to be kept warm after being heated, the induction heating system will switch to the inner-loop power supply mode. At this moment, the left-side transistors of the inverter will be composed of Q_1 and Q_3. The input power V_{in} is converted into a high-frequency square wave by switching Q_1 and Q_3 and applied in the resonant circuit of the inner heating coil and its compensation capacitor, and then the energy of the resonant circuit is induced to heat the inner part of the heated load. Because of the mutual inductance between the inner and outer coils, a current will also be induced in the outer coil to heat the outer area of the load. To sum up, this system operates in different power supply modes by switching among different circuits. Through switching, this system adjusts the heating areas for various heating needs. The proposed system further incorporates the mutual inductance between the inner and the outer coils, to retain part of the heating effect even when the coil is not powered. This further helps the uniform heat distribution.

In the following, the coil structure is described in this section. Figure 2 illustrates the coaxial dual-loop coil and load placement. The coil structure is composed of an inner coil and an outer coil. The inner coil and the outer coil are wound in a coaxial and concentric rectangular form. Figure 2(a) and Figure 2(b) are the actual photos of the outer heating coil and the inner heating coil, respectively, and both coils are made of Litz wire with a diameter of 0.1mm at a total of 240 strands. Moreover, considering the size of the commonly used cookware on the market is about 16 cm to 22 cm in diameter, which constitutes a major factor for coil size design in this paper, the diameter of the outer heating coil is about 20 cm, and that of the inner heating coil is about 10 cm as shown in Figure 2(c).

The inner and outer heating coils are wound coaxially and placed on the same surface to achieve effective heating. Finally, to prevent the insulation part of the coil from being burned out when the temperature of the heating load rises and causes a short circuit of the coils, the distance between the heating load and both coils is set to be 2 cm. The heat load material is made of SAE 304 stainless steel, a common material for household cookware.

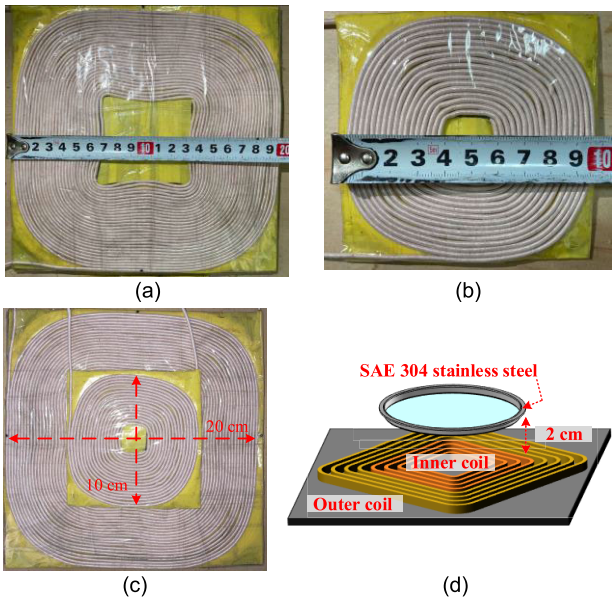

FIGURE 2. Schematic diagrams for coaxial dual coils and load placement.

TABLE 1. Symbol table.

Symbol	Description
V_{in}	Input voltage, Input power
$Q_1 \sim Q_5$	Power transistors of composite bridge-type inverter
$I_{Q1} \sim I_{Q5}$	The current flowing through power transistors
v_m	Voltage across the outer coil and its compensating circuit
v_t	Voltage across the inner coil and its compensating circuit
i_m	Current of the outer coil and its compensating circuit
i_t	Current of the inner coil and its compensating circuit
L_m	Resonant inductance of the outer heating coil
L_t	Resonant inductance of the inner heating coil
C_m	Resonant capacitance of the outer heating coil
C_t	Resonant capacitance of the inner heating coil
R_m	Equivalent resistor of the outer heating coil
R_t	Equivalent resistor of the inner heating coil
M_{mt}	Mutual inductance of dual heating coils

III. CIRCUIT TIME WAVEFORM ANALYSIS

Since the coaxial dual-loop coil and composite bridge induction heating circuit proposed can switch among different power supply modes according to different heating needs, this section will provide detailed descriptions of the circuit actions in different power supply modes by using corresponding time waveforms. The following will analyze and explain the power transistor switching duty cycles, voltages, and currents during the three power supply modes using the time waveforms and circuit action diagrams. The symbols and their explanations are listed for various components, voltages, and currents in the following table:

A. MODE A. DUAL-LOOP POWER SUPPLY MODE

1) PHASE D_1 ($t_0 \sim t_1$)

Figure 3 and Figure 4 are the circuit timing waveform diagrams and circuit action schematic diagrams of the dual-loop power supply mode respectively. As shown during the period $t_0 \sim t_1$ in Figure 3 and Figure 4(a), Q_1, Q_2, and Q_5 are all on, and Q_3 and Q_4 are both turned off. The voltage drops across Q_1 and Q_5 are zero, while I_{Q1} and I_{Q5} are negative and rise gradually, and flow through their body diodes. Therefore, in this phase, zero voltage switching (ZVS) is achieved when Q_1 and Q_5 are turned on. The current i_t flowing through the inner coil and its compensation circuit is negative, and a conducting path is formed by Q_1, V_{in}, L_t, C_t, and Q_2 for i_t. The current i_m flowing through the outer coil and its compensation circuit is also negative, and this conducting path is formed by Q_1, V_{in}, Q_5, C_m, and L_m. Phase D_1 is completed when i_t rises to zero, and the system enters phase D_2.

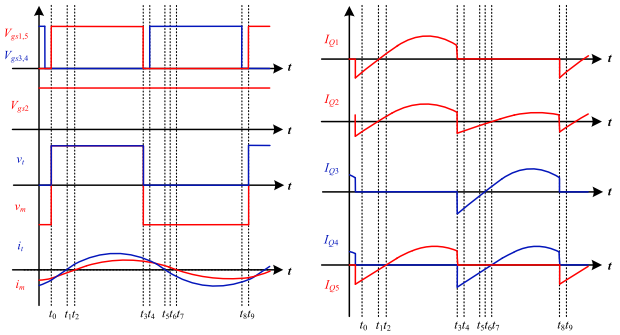

FIGURE 3. Time waveforms in dual-loop power supply mode.

2) PHASE D_2($t_1 \sim t_2$)

In this working phase, as illustrated in the $t_1 \sim t_2$ period in Figure 3 and Figure 4(b), Q_1, Q_2, and Q_5 are all turned on, and Q_3 and Q_4 are turned off. Since i_t turns from zero to positive and continues to rise during this period, I_{Q1} and I_{Q2} also increase from zero to positive and continue to rise. A conducting path is formed for i_t consisting of Q_1, Q_2, C_t, L_t, and V_{in}. While i_m remains negative, its conducting path is formed by L_m, Q_2, C_t, L_t, Q_5, and C_m. It marks the end of working phase D_2 when i_m rises to zero. The system then proceeds to phase D_3.

3) PHASE D_3($t_2 \sim t_3$)

During phase D_3, as shown in $t_2 \sim t_3$ in Figure 3 and Figure 4(c), Q_1, Q_2, and Q_5 are all turned on and Q_3 and Q_4 are off. Since i_m rises from zero to positive and I_{Q5} also rises from zero to positive. At this moment, i_t is positive, and its conducting path is formed by L_t, V_{in}, Q_1, Q_2, and C_t. A conducting path for i_m which consists of L_m, Q_5, V_{in}, and Q_1 is formed. Phase D_3 continues until Q_1 and Q_5 are cut off. Subsequently, the system embarks on phase D_4.

4) PHASE D_4($t_3 \sim t_4$)

In this phase, as shown in the $t_3 \sim t_4$ period in Figure 3 and Figure 4(d), Q_2 is turned on, and Q_1, Q_3, Q_4, and Q_5 are off. Because no energy can be passed to the circuits of the inner or the outer coils from V_{in} through any power transistors,

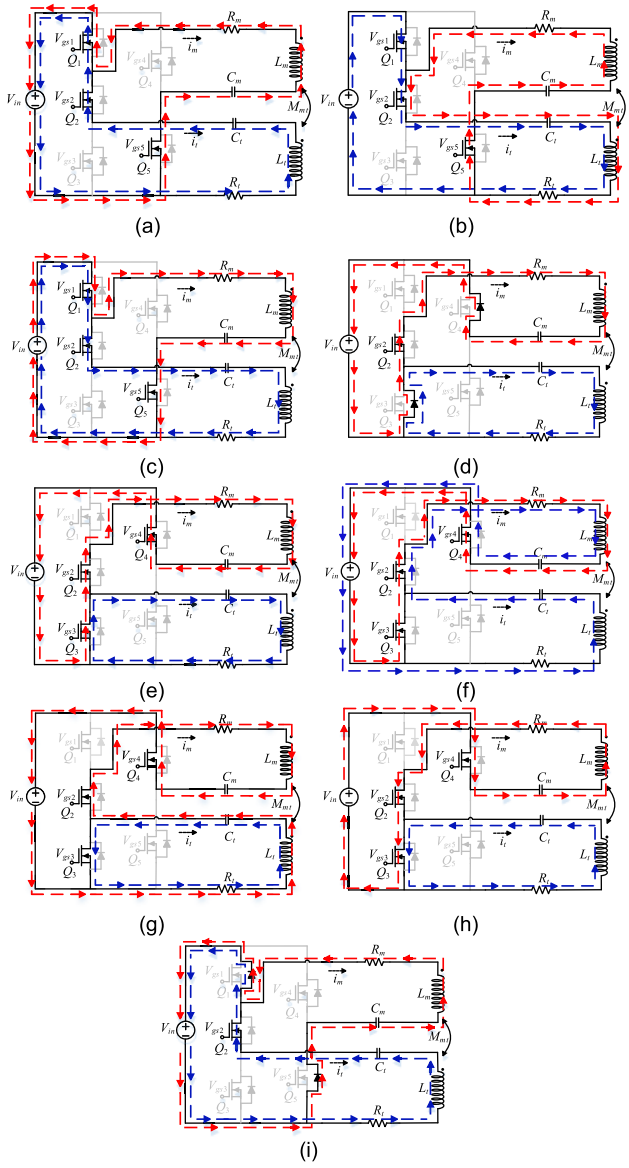

FIGURE 4. Circuit actions schematics for dual-loop power supply mode, (a) $t_0 \sim t_1$, (b) $t_1 \sim t_2$, (c) $t_2 \sim t_3$, (d) $t_3 \sim t_4$, (e) $t_4 \sim t_5$, (f) $t_5 \sim t_6$, (g) $t_6 \sim t_7$, (h) $t_7 \sim t_8$, and (i) $t_8 \sim t_9$.

this period is called dead time. At this moment, I_{Q1} and I_{Q5} become zero because Q_1 and Q_5 are turned off. Q_2 is continuously turned on, but the passing current of Q_2 switches from i_t to i_m. Hence, I_{Q2} turns from positive to negative, and the parasitic capacitances of Q_3 and Q_4 discharge, so I_{Q3} and I_{Q4} gradually increase from negative. Since i_t and i_m are both continuously positive, a conducting path for i_t is formed through L_t, the body diode of Q_3, and C_t. Another conducting path for i_m composed of L_m, C_m, the body diode of Q_4, V_{in}, the body diode of Q_3, and Q_2 is formed. This phase continues until Q_3 and Q_4 are turned on, which will mark the beginning of working phase D_5.

5) PHASE $D_5(t_4 \sim t_5)$

In phase D_5, as shown in the period $t_4 \sim t_5$ in Figure 3 and Figure 4(e), Q_2, Q_3, and Q_4 are turned on, while Q_1 and Q_5 are turned off. Since the voltages across Q_3 and Q_4 drop to zero in phase D4, while I_{Q3} and I_{Q4} are negative and rise gradually, and flow through the body diodes of Q_3 and Q_4. Therefore, the ZVS is achieved when Q_3 and Q_4 are turned on in this phase. In this instant, i_t and i_m are still positive. Hence, a conducting path for it is formed by L_t, Q_3, and C_t. Another conducting path for i_m consisting of L_m, C_m, Q_4, V_{in}, Q_3, and Q_2 is formed. When it drops to zero, phase D_5 ends and the system enters phase D_6.

6) PHASE $D_6(t_5 \sim t_6)$

In this phase, as shown in the $t_5 \sim t_6$ period in Figure 3 and Figure 4(f), Q_2, Q_3, and Q_4 are all turned on, while Q_1 and Q_5 are off. At this point, because i_m is still positive and passes through Q_3, I_{Q3} rises from negative to zero. Meanwhile, i_t turns from positive to negative, and a conducting path for i_t is formed through L_t, C_t, Q_2, L_m, C_m, Q_4, and V_{in}. Also, since i_m is gradually decreasing, a conducting path is formed for i_m by L_m, C_m, Q_4, V_{in}, Q_3, and Q_2, until the power transistor current I_{Q3} rises to zero. Phase D_6 is then completed and phase D_7 begins.

7) PHASE $D_7(t_6 \sim t_7)$

In phase D_7, as shown in the $t_6 \sim t_7$ period in Figure 3 and Figure 4(g), Q_2, Q_3, and Q_4 are turned on, while Q_1 and Q_5 are turned off. At this point, because Q_3 is continuously turned on and its passing current changes from i_m to i_t, with i_t being negative, so I_{Q3} turns from zero to positive and gradually rises. A conducting path for i_t is formed by L_t, C_t, and Q_3. i_m is positive and a conducting path for i_m is formed through L_m, C_m, Q_4, V_{in}, L_t, C_t, and Q_2. Phase D_7 ends and phase D_8 begins when i_m drops to zero.

8) PHASE $D_8(t_7 \sim t_8)$

In phase D_8, Q_2, Q_3, and Q_4 are turned on, while Q_1 and Q_5 are switched off, as illustrated in the $t_7 \sim t_8$ period in Figure 3 and Figure 4(h). At this point, because Q_4 is turned on and its passing current i_m keeps decreasing from zero, therefore, I_{Q4} keeps increasing from zero. In this instant, i_t is still negative, a conducting path for i_t is formed by L_t, C_t, and Q_3. Further, i_m turns from zero to negative, and a conducting path is formed by L_m, Q_2, Q_3, V_{in}, Q_4, and C_m. This phase continues till Q_3 and Q_4 are cut off, which also marks the beginning of phase D_9.

9) PHASE $D_9(t_8 \sim t_9)$

In this phase, as shown in the $t_8 \sim t_9$ period in Figure 3 and Figure 4(i), Q_2 is turned on, while Q_1, Q_3, Q_4, and Q_5 are all turned off. Since no energy can be delivered to the circuits of the inner or the outer coils from V_{in} through any power transistors. Hence, this period is called dead time. In addition, I_{Q3} and I_{Q4} change from positive to zero due to the cut-off of Q_3 and Q_4. While Q_2 is continuously turned on, the current passing through changes from i_m to i_t. Thus, I_{Q2} turns from positive to negative. Further, the parasitic capacitances of Q_1 and Q_5 are discharged, so the negative currents I_{Q1} and I_{Q5}

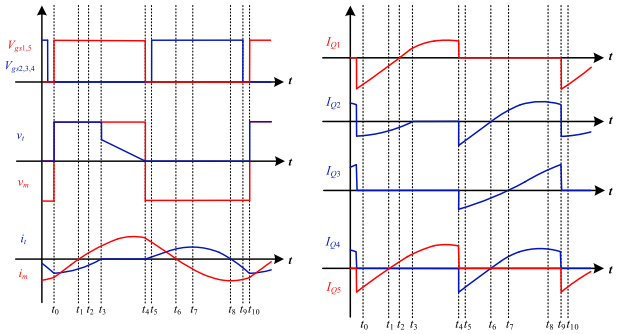

FIGURE 5. Time waveforms in outer loop power supply mode.

continue decreasing. Since i_t and i_m are both negative and continue to flow, it forms a conducting path for i_t through L_t, C_t, Q_2, the body diode of Q_1, and V_{in}. Another conducting path consisting of L_m, the body diode of Q_1, V_{in}, the body diode of Q_5, and C_m is formed for i_m. This phase continues until Q_1 and Q_5 are turned on and the system returns to phase D_1 to repeat.

B. MODE B. OUTER LOOP POWER SUPPLY MODE

1) PHASE O_1 ($t_0 \sim t_1$)

Figure 5 and Figure 6 are respectively the circuit time waveforms and circuit action schematic diagrams during the outer loop power supply mode. As shown in Figure 5 during $t_0 \sim t_1$ and Figure 6 (a), Q_1 and Q_5 are both turned on, and Q_2, Q_3, and Q_4 are all cut off. In the previous phase, the voltage across Q_1 and Q_5 are both zero, while I_{Q1} and I_{Q5} are negative and rise gradually, flowing through body diodes of Q_1 and Q_5. Therefore, in this phase, the ZVS is achieved when Q_1 and Q_5 are turned on. i_m flowing through the outer coil and its compensation circuit is negative, and a conducting path is formed by Q_1, V_{in}, Q_5, C_m, and L_m for i_m. i_t flowing through the inner coil and its compensation circuit is also negative, and a conducting path is formed by Q_1, V_{in}, L_t, C_t, and the body diode of Q_2. Phase O_1 continues until i_m rises to zero, which also marks the beginning of phase O_2.

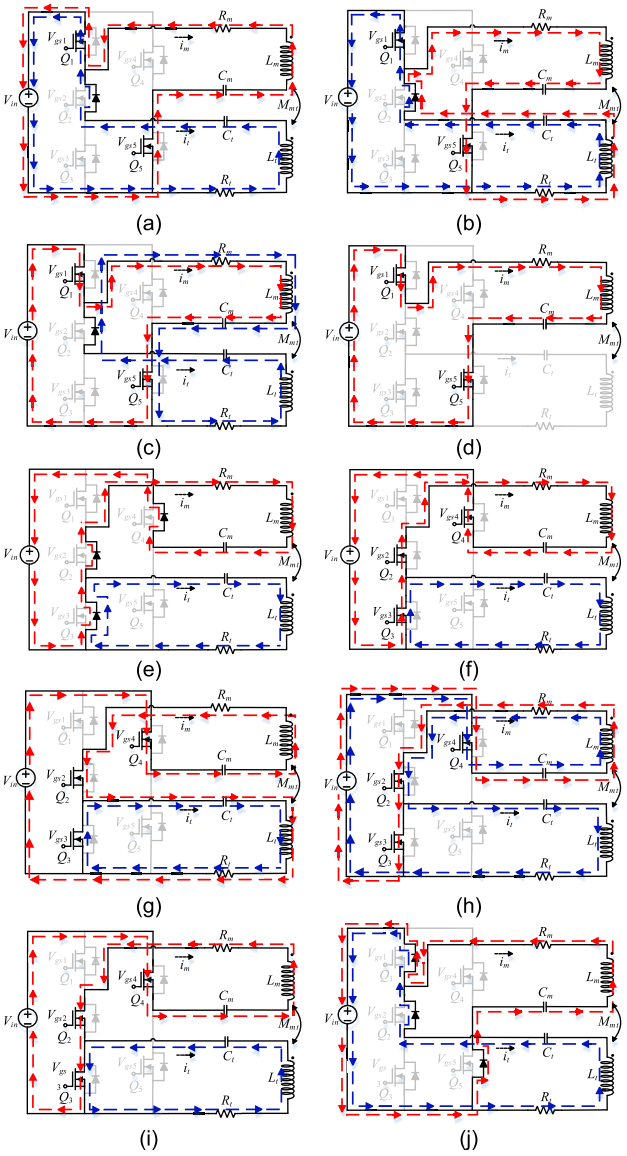

FIGURE 6. Circuit actions schematics for outer loop power supply mode, (a) $t_0 \sim t_1$, (b) $t_1 \sim t_2$, (c) $t_2 \sim t_3$, (d) $t_3 \sim t_4$, (e) $t_4 \sim t_5$, (f) $t_5 \sim t_6$, (g) $t_6 \sim t_7$, (h) $t_7 \sim t_8$, (i) $t_8 \sim t_9$, and (j) $t_8 \sim t_9$.

2) PHASE O_2 ($t_1 \sim t_2$)

In phase O_2, Q_1 and Q_5 are both turned on, and Q_2, Q_3, and Q_4 are all turned off as shown in the period $t_1 \sim t_2$ in Figure 5 and Figure 6(b). Since i_m continues to rise from zero to positive, I_{Q5} also continues to rise from zero. i_m passes through L_m, C_m, Q_5, L_t, C_t, and the body diode of Q_2, which constitute a conducting path. While i_t is still negative in value, a conducting path is formed through L_t, C_t, the body diode of Q_2, Q_1, and V_{in}. This phase continues till I_{Q1} rises to zero which concludes phase O_2 and starts phase O_3.

3) PHASE O_3 ($t_2 \sim t_3$)

In phase O_3, Q_1 and Q_5 are both on, and Q_2, Q_3, and Q_4 are off as shown in the period $t_2 \sim t_3$ in Fig. 5 and Fig. 6(c). At this point, Q_1 continues to be turned on, while its passing current changes from i_t to i_m. i_m continues to rise, so I_{Q1} turns from zero to positive and gradually rises. A conducting path for i_m consisting of L_m, C_m, Q_5, V_{in}, and Q_1 is formed. i_t is negative, and its conducting path is formed through L_t, C_t, the body diode of Q_2, L_m, C_m, and Q_5. This phase continues until i_t rises to zero. This marks the end of Phase O_3 and starts Phase O_4.

4) PHASE O_4($t_3 \sim t_4$)

In this phase, as illustrated in the period $t_3 \sim t_4$ in Fig. 5 and Fig. 6(d), Q_1 and Q_5 are both on, and Q_2, Q_3, and Q_4 are off. Meanwhile, I_{Q1} and I_{Q5} are also positive and continue to rise, and the other currents I_{Q2}, I_{Q3}, and I_{Q4} are zero because i_m is positive and continues to rise and i_t is zero. i_m has a

conducting path composed of L_m, C_m, Q_5, V_{in}, and Q_1. This phase continues until Q_1 and Q_5 are cut off to complete phase O_4 and start phase O_5.

5) PHASE $O_5(t_4 \sim t_5)$

In this phase, as shown in the $t_4 \sim t_5$ period in Figure 5 and Figure 6(e), all power transistors are cut off. Because the input power source (V_{in}) is unable to deliver energy to either the inner or outer coil through any power transistor, this period is usually called dead time. At this moment, I_{Q1} and I_{Q5} become zero because Q_1 and Q_5 are turned off. Since the parasitic capacitances of Q_2, Q_3, and Q_4 are discharged, I_{Q2}, I_{Q3}, and I_{Q4} gradually rise from negative. Note that i_t and i_m are both positive and continuously flowing, L_m, C_m, the body diode of Q_4, V_{in}, and the body diodes of Q_3 and Q_2 form a conducting path for i_m. Another conducting path is formed by L_t, the body diode of Q_3, and C_t for i_t. Phase O_5 concludes when Q_2, Q_3, and Q_4 are turned on, which also marks the beginning of phase O_6.

6) PHASE $O_6(t_5 \sim t_6)$

In this phase, as shown during $t_5 \sim t_6$ in Figure 5 and Figure 6(f), Q_2, Q_3, and Q_4 are turned on, while Q_1 and Q_5 are off. In phase O5, because the voltage across Q_2, Q_3, and Q_4 are zero, while I_{Q2}, I_{Q3}, and I_{Q4} are negative, gradually increasing and flowing through body diodes of Q_2, Q_3, and Q_4. Thus, ZVS is achieved in Q_2, Q_3, and Q_4. Meanwhile, i_m is positive and continues to decrease. A conducting path is formed through L_m, C_m, Q_4, V_{in}, Q_3, and Q_2 for i_m. Further, the load is heated. Another conducting path is formed through L_t, Q_3, and C_t for i_t. Until i_m drops to zero to complete phase O_6. This also starts phase O_7.

7) PHASE $O_7(t_6 \sim t_7)$

In phase O_7, as shown in the $t_6 \sim t_7$ period in Figure 5 and Figure 6(g), Q_2, Q_3, and Q_4 are turned on, while Q_1 and Q_5 are off. I_{Q2} and I_{Q4} turn from zero to positive and continue to rise because i_m turns from zero to negative. A conducting path for i_m consists of L_m, Q_2, C_t, L_t, V_{in}, Q_4, and C_m. Another conducting path is formed by L_t, Q_3, and C_t for i_t. This phase continues until I_{Q3} rises to zero to complete phase O_7. Subsequently, the system proceeds to phase O_8.

8) PHASE $O_8(t_7 \sim t_8)$

In this phase, as shown in the $t_7 \sim t_8$ period in Figure 5 and Figure 6(h), Q_2, Q_3, and Q_4 are turned on, and Q_1 and Q_5 are turned off. At this moment, because Q_3 is continuously turned on while its passing current changes from i_t to i_m. Moreover, i_m continues to be negative. Hence, I_{Q3} turns from zero to positive and gradually rises. A conducting path of i_m consisting of L_m, Q_2, Q_3, V_{in}, Q_4, and C_m is formed. For i_t, this conducting path is formed by L_t, V_{in}, Q_4, C_m, L_m, Q_2, and C_t. Phase O_8 ends when i_t drops to zero. This also starts phase O_9.

9) PHASE $O_9(t_8 \sim t_9)$

In phase O_9, as shown in the $t_8 \sim t_9$ period in Figure 5 and Figure 6(i), Q_2, Q_3, and Q_4 are turned on, while Q_1 and Q_5 are off. At this moment, i_t changes from zero to negative, while Q_3 is continuously turned on and its passing currents are i_t and i_m, thus, I_{Q3} rises quickly. In addition, because Q_2 and Q_4 are continuously turned on, and the passing current switches to i_m, the increase of I_{Q2} and I_{Q4} subside. L_m, Q_2, Q_3, V_{in}, Q_4, and C_m form a conducting path for i_m. Another conducting path for i_t is formed by L_t, C_t, and Q_3. Phase O_9 ends when Q_2, Q_3, and Q_4 are cut off, which also starts phase O_{10}.

10) PHASE $O_{10}(t_9 \sim t_{10})$

In phase O_{10}, as shown in $t_9 \sim t_{10}$ in Figure 5 and Figure 6(j), all power transistors are turned off. Because the input power source (V_{in}) cannot deliver energy through any power transistors to either the inner or the outer coil, this period is called dead time. At this moment, I_{Q3} and I_{Q4} become zero because Q_3 and Q_4 are turned off. The current passing through Q_2 changes from i_m to i_t. Thus, I_{Q2} turns from positive to negative, and the parasitic capacitances of Q_1, Q_2, and Q_5 are discharged. I_{Q1}, I_{Q2}, and I_{Q5} gradually increase from negative values as a result. Because i_t and i_m are both negative and continue to flow, a conducting path of i_m is formed by L_m, the body diode of Q_1, V_{in}, the body diode of Q_5, and C_m. Another conducting path for i_t is formed by L_t, C_t, the body diodes of Q_2 and Q_1, and V_{in}. This phase concludes when Q_1 and Q_5 are turned on again. This system will return to phase O_1 and repeat the process.

C. MODE C. INNER LOOP POWER SUPPLY MODE

1) PHASE I_1 ($t_0 \sim t_1$)

Figure 7 shows the time waveforms of voltages and currents, while Figure 8 is the circuit action schematic diagram of the inner loop power supply mode. As shown in the $t_0 \sim t_1$ period in Figure 7 and Figure 8 (a), Q_1 and Q_2 are turned on, and Q_3, Q_4, and Q_5 are off. In the previous phase, the voltages across Q_1 and Q_2 are zero, and I_{Q1} and I_{Q2} are negative, gradually rising and flowing respectively through their body diodes. Therefore, in this phase, ZVS is completed in Q_1 and Q_2. The current i_t of the inner coil and its compensation circuit is negative, and a conducting path for i_t is formed through Q_1, V_{in}, L_t, C_t, and Q_2. The current i_m passing through the outer coil and its compensation circuit is also negative, and a conducting path for i_m is formed by Q_1, V_{in}, the body diode of Q_5, C_m, and L_m. Phase I_1 ends when i_t rises and reaches zero. This also marks the beginning of phase I_2.

2) PHASE I_2 ($t_1 \sim t_2$)

In this phase, as shown in the $t_1 \sim t_2$ period in Figure 7 and Figure 8(b), Q_1 and Q_2 are turned on, while Q_3, Q_4 and Q_5 are off. Since i_t turns from zero to positive at this moment and continues to rise, I_{Q2} also turns from zero to positive and continues to rise. A conducting path for i_t is formed by Q_2, C_t, L_t, the body diode of Q_5, C_m, and C_m. Meanwhile, i_m is still

negative, a conducting path is formed by Q_1, V_{in}, the body diode of Q_5, C_m, and L_m. This phase ends when I_{Q1} rises to zero, which also marks the beginning of phase I_3

3) PHASE $I_3(t_2 \sim t_3)$

In phase I_3, as shown in the $t_2 \sim t_3$ period in Figure 7 and Figure 8(c), Q_1 and Q_2 are turned on, while Q_3, Q_4, and Q_5 are off. Q_1 is continuously turned on, while the passing current changes from i_m to i_t. Hence, I_{Q1} turns from zero to positive and i_t continues to be positive and rising. Moreover, a conducting path for i_t is formed through L_t, V_{in}, Q_1, Q_2, and C_t. However, i_m is still negative and continues to rise. A conducting path for i_m is formed through L_m, Q_2, C_t, L_t, the body diode of Q_5, and C_m. Phase I_3 ends when i_m rises to zero, which also embarks on phase I_4.

4) PHASE $I_4(t_3 \sim t_4)$

In this phase, as shown in the period $t_3 \sim t_4$ in Figure 7 and Figure 8(d), Q_1 and Q_2 are turned on, while Q_3, Q_4, and Q_5 continue to be off. Since i_m starts to rise from zero to positive at this moment, its current flows from the body diode of Q_5 to the body diode of Q_4, so I_{Q5} is zero and I_{Q4} starts to turn from zero to negative. In this instant, i_t continues to be positive and starts to decrease. A conducting path for i_t is formed by L_t, V_{in}, Q_1, Q_2, and C_t. Meanwhile, a conducting path of i_m is formed by Q_1, L_m, C_m, and the body diode of Q_4. This phase ends when Q_1 is cut off. Subsequently, phase I_5 starts.

5) PHASE $I_5(t_4 \sim t_5)$

In this phase, as illustrated in the $t_4 \sim t_5$ period in Figure 7 and Figure 8(e), Q_2 is turned on, while Q_1, Q_3, Q_4, and Q_5 are all off. Since the input cannot deliver energy to either the inner or the outer coil, this period is called idle time. At this moment, I_{Q1} becomes zero because Q_1 is turned off. However, Q_2 continues to be turned on with the passing current changes from i_t to i_m. Hence, I_{Q2} turns from positive to negative, and the parasitic capacitance of Q_3 is discharged, therefore, I_{Q3} gradually rises from negative. Since both i_t and i_m are positive and flow continuously, a conducting path for i_t is formed by L_t, the body diode of Q_3, and C_t. Further, a conducting path for i_m is formed by a conducting path by L_m, C_m, the body diode of Q_4, V_{in}, the body diode of Q_3, and Q_2. This phase ends when Q_3 is turned on, which also starts phase I_6.

6) PHASE $I_6(t_5 \sim t_6)$

In this phase, as illustrated in $t_5 \sim t_6$ in Figure 7 and Figure 8(f), Q_2 and Q_3 are turned on, while Q_1, Q_4 and Q_5 are all off. Because during phase I5, the voltage drop across Q_3 is zero, I_{Q3} is negative and gradually rising. Thus, Q_3 achieves zero-voltage switching (ZVS). Meanwhile, both the inner and outer coils current i_t and i_m are positive, a conducting path for i_t is formed by L_t, Q_3, and C_t. A conducting path is formed for i_m which consists of L_m, C_m, the body diode of Q_4, V_{in}, Q_3, and Q_2. Phase I_6 concludes when i_t drops to zero, which also commences phase I_7.

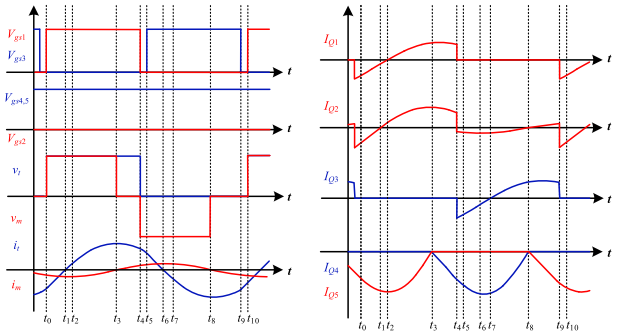

FIGURE 7. Time waveforms in inner loop power supply mode.

7) PHASE $I_7(t_6 \sim t_7)$

In this phase, as indicated in $t_6 \sim t_7$ in Figure 7 and Figure 8(g), Q_2 and Q_3 are turned on, while Q_1, Q_4, and Q_5 are off. Since i_t turns from zero to negative, a conducting path is formed for i_t by L_t, C_t, Q_2, L_m, C_m, the body diode of Q_4, and V_{in}. A conducting path is formed for i_m which consists of L_m, C_m, the body diode of Q_4, V_{in}, Q_3, and Q_2. Phase I_7 ends when I_{Q3} rises to zero, which also marks the beginning of phase I_8.

8) PHASE $I_8(t_7 \sim t_8)$

In phase I_8, as shown in $t_7 \sim t_8$ in Figure 7 and Figure 8(h), Q_2 and Q_3 are turned on, while Q_1, Q_4 and Q_5 are off. In this instant, because Q_3 is continuously turned on and its passing current changes from i_m to i_t, and i_t continues to be negative, so I_{Q3} turns from zero to positive and rises gradually. A conducting path for i_t is formed by L_t, C_t, and Q_3. A conducting path for i_m is formed by L_m, C_m, the body diode of Q_4, V_{in}, L_t, C_t, and Q_2. This phase ends when i_m drops to zero, which also marks the beginning of phase I_9.

9) PHASE $I_9(t_8 \sim t_9)$

In this phase, as shown in the period $t_8 \sim t_9$ in Figure 7 and Figure 8(i), Q_2 and Q_3 are turned on, while Q_1, Q_4, and Q_5 are off. At this moment, i_m turns from zero to negative, i_t is negative and starts to rise, Q_2 is continuously turned on and its passing current is i_m, so I_{Q2} turns from zero to positive. Q_3 is also continuously turned on, with its passing current being i_t and i_m, so the increase of I_{Q3} is slowed down. In addition, due to the change of direction of the i_m, the current changes in the route from the body diode of Q_4 to flowing through the body diode of Q_5, so I_{Q4} is zero and I_{Q5} starts to turn from zero to negative. A conducting path for i_t is formed by L_t, C_t, and Q_3. A conducting path is formed for i_m by L_m, Q_2, Q_3, the body diode of Q_5, C_m. This phase ends when Q_3 is cut off, which also starts phase I_{10}.

10) PHASE I_{10} $(t_9 \sim t_{10})$

In this phase, as shown in the $t_9 \sim t_{10}$ period in Figure 7 and Figure 8(j), Q_2 is turned on, and Q_1, Q_3, Q_4, and Q_5 are all off. Because the input cannot deliver power to either the

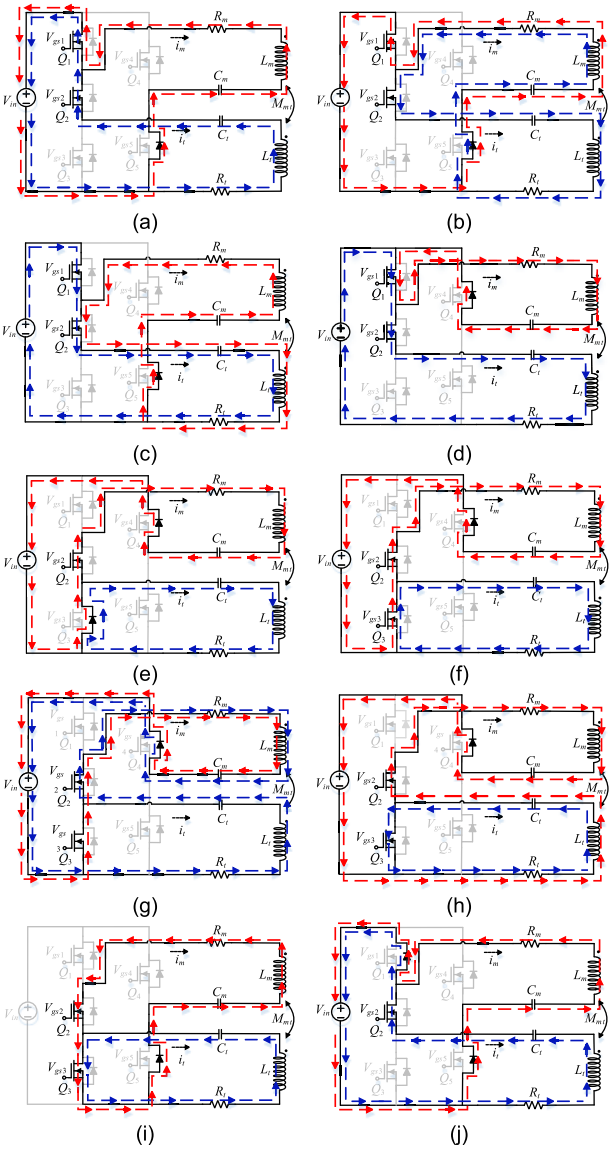

FIGURE 8. Circuit actions schematics for inner loop power supply mode, (a) $t_0 \sim t_1$, (b) $t_1 \sim t_2$, (c) $t_2 \sim t_3$, (d) $t_3 \sim t_4$, (e) $t_4 \sim t_5$, (f) $t_5 \sim t_6$, (g) $t_6 \sim t_7$, (h) $t_7 \sim t_8$, (i) $t_8 \sim t_9$, and (j) $t_8 \sim t_9$.

inner or the outer coil, this period is called idle time. In this instant, I_{Q3} becomes zero because Q_3 is turned off, while Q_2 remains turned on with the passing current changes from i_m to i_t. Hence, I_{Q2} turns from positive to negative, and the parasitic capacitance of Q_1 is discharged. Moreover, the current of I_{Q1} gradually increases from negative. Since i_t and i_m continue to flow and are both negative, a conducting path is formed for i_t by L_t, C_t, Q_2, the body diode of Q_1, and V_{in}. A conducting path for i_m consisting of L_m, the body diode of Q_1, V_{in}, the body diode of Q_5, and C_m is formed. This phase is concluded when Q_1 is turned on again. Subsequently, the process returns to phase I_1 to repeat.

IV. RESONANT CIRCUIT ANALYSIS

To optimize the heating efficiency, this paper will carry out parameter analysis for the coaxial dual-loop coil with

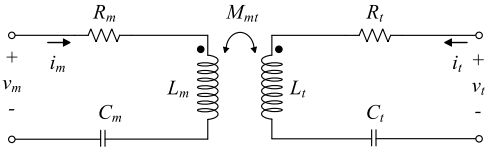

FIGURE 9. Dual series resonance equivalent circuit diagram.

a double series resonant architecture circuit. Because the composite bridge-type inverter circuit proposed in this article is combined with the coaxial dual-loop coil to switch the heating modes, and then achieve the maximum power output by aligning the magnetic field with ferrite. Therefore, this section starts with an analysis of the dual-loop power supply mode and then checks if the resonance parameters calculated in this mode, are appropriate for the outer loop power supply mode and the inner loop power supply mode. The main reason is that during the heating process, the dual-loop power supply mode is the main mode of operation, the inner loop power supply and the outer loop power supply are subsidiaries during the heating process. Therefore, the circuit parameters for the dual loop power supply mode must be used to ensure its parameters are suitably chosen to achieve optimal heating performance. Figure 9 is the dual series resonance equivalent circuit diagram used in this paper. Some heating effects are achieved through mutual inductance, and the reheating can be made more quickly through the coil warmth preservation effect.

Here, L_m and C_m are the resonant inductance and resonant compensation capacitor of the outer heating coil. L_t and C_t are the resonant inductance and resonant compensation capacitor of the inner heating coil. R_m and R_t are the corresponding heating load equivalent resistance of the outer heating coil and the inner heating coil. M_{mt} is the mutual inductance between the outer heating coil and the inner heating coil. According to Kirchhoff's voltage law, the loop equation is as follows:

$$v_m = i_m \left(R_m + j\omega L_m + \frac{1}{j\omega C_m} \right) + i_t \left(j\omega M_{mt} \right) \tag{1}$$

$$v_t = i_m \left(j\omega M_{mt} \right) + i_t \left(R_t + j\omega L_t + \frac{1}{j\omega C_t} \right) \tag{2}$$

Simplifying equations (1) and (2) facilitates subsequent calculation of the compensation capacitance, this section expresses the equivalent impedance of the inner coil, the resonance compensation capacitance, and its equivalent resistance as Z_t, while the equivalent impedance of the outer coil, the resonance compensation capacitance, and its equivalent resistance is represented by Z_m, as shown in the following formula:

$$\begin{cases} Z_t = R_t + j\omega L_t + \dfrac{1}{j\omega C_t} \\ Z_m = R_m + j\omega L_m + \dfrac{1}{j\omega C_m} \end{cases} \tag{3}$$

By using (1), (2) and (3), the parameters of the loop equation are expressed in terms of an inverse matrix as (4). The current i_m of the outer heating coil and inner heating coil current i_t can be obtained by formula (4) in the following:

$$\begin{bmatrix} i_m \\ i_t \end{bmatrix} = \begin{bmatrix} Z_m & j\omega M_{mt} \\ j\omega M_{mt} & Z_t \end{bmatrix}^{-1} \begin{bmatrix} v_m \\ v_t \end{bmatrix} = \begin{bmatrix} \frac{Z_t}{Z_m Z_t + \omega^2 M_{mt}^2} & \frac{-j\omega M_{mt}}{Z_m Z_t + \omega^2 M_{mt}^2} \\ \frac{-j\omega M_{mt}}{Z_m Z_t + \omega^2 M_{mt}^2} & \frac{Z_m}{Z_m Z_t + \omega^2 M_{mt}^2} \end{bmatrix} \begin{bmatrix} v_m \\ v_t \end{bmatrix} \quad (4)$$

$$i_m = \frac{v_m Z_t - j v_t \omega M_{mt}}{Z_m Z_t + \omega^2 M_{mt}^2} \quad (5)$$

$$i_t = \frac{v_t Z_m - j v_m \omega M_{mt}}{Z_m Z_t + \omega^2 M_{mt}^2} \quad (6)$$

The voltage and current of the inner and outer coils have been derived respectively. Since the coaxial dual-loop coil is used in this paper, the influence of the dual-loop coil and its mutual inductance on the equivalent impedance must be considered. Therefore, to consider the equivalent input impedance of the dual loop and its mutual inductance, the voltage and current of the inner and outer loop coils are calculated to obtain the following:

$$Z_{m\_in} = \frac{v_m}{i_m} = \frac{v_m Z_m Z_t + \omega^2 v_m M_{mt}^2}{v_m Z_t - j v_t \omega M_{mt}} \quad (7)$$

$$Z_{t\_in} = \frac{v_t}{i_t} = \frac{v_t Z_m Z_t + \omega^2 v_t M_{mt}^2}{v_t Z_m - j v_m \omega M_{mt}} \quad (8)$$

It can be observed from (7) and (8) that there must be three parameters of Z_m, Z_t, and M_{mt} in the equivalent input impedance Z_{t_in} and Z_{m_in}. Which means that not only the independent equivalent load is considered, but the influence of mutual inductance also needs to be considered in the calculation of equivalent impedance. However, it is impossible to compute an appropriate inner and outer coil resonance compensation capacitance at the same time. Therefore, to establish a successful coaxial dual-loop coil resonance structure, the resonance compensation capacitor method in one of the heating coils must be selected first, then the resonance compensation capacitor of the other heating coil based on the calculated parameters of the selected resonant compensation capacitor along with its resonance characteristics. Here, the compensation capacitance of the outer coil is set first as shown in Figure 10, which shows the equivalent circuit diagram of the outer coil, its resonant compensation capacitor and equivalent resistance. Further, (9) is established according to Kirchhoff's voltage law and followed by the impedance derivation in (10).

$$v_m = i_m \left(R_m + j\omega L_m + \frac{1}{j\omega C_m} \right) \quad (9)$$

$$Z_m = R_m + j \left(\omega L_m - \frac{1}{\omega C_m} \right) \quad (10)$$

To optimize the heating effect, the imaginary part of the impedance must be set to zero for impedance matching as

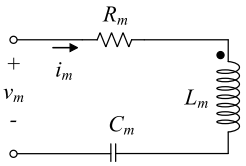

FIGURE 10. Equivalent circuit of the outer-loop coil.

shown in (11). The resonant compensation capacitor C_m is deduced from (11) as shown in (12):

$$0 = \omega L_m - \frac{1}{\omega C_m} \quad (11)$$

$$C_m = \frac{1}{\omega^2 L_m} \quad (12)$$

From the above equation, the resonance compensation capacitance of the outer coil can be obtained, and its parameter value can be set. Next, consider the construction of the dual-loop heating coil, the compensation capacitance obtained from merely the coil of the outer loop is substituted back to the input impedance Z_{t_in} of the inner loop that has considered the influence of the dual-loop and mutual inductance. Hence, C_m is substituted back to (8) as follows:

$$\begin{aligned} Z_{t\_in} &= \frac{v_t \left(R_m Z_t + \omega^2 M_{mt}^2 \right)}{v_t R_m - j\omega M_{mt} v_m} \\ &= \frac{\left[v_t \left(R_m Z_t + \omega^2 M_{mt}^2 \right) \right] \left(v_t R_m + j\omega M_{mt} v_{mt} \right)}{\left(v_t R_m - j\omega M_{mt} v_{mt} \right) \left(v_t R_m + j\omega M_{mt} v_{mt} \right)} \\ &= \frac{v_t^2 R_m^2 Z_t + \omega^2 M_{mt}^2 v_t^2 R_m}{v_t^2 R_m^2 + \omega^2 v_m^2 M_{mt}^2} \\ &\quad + \frac{j\omega \left(v_m v_t R_m M_{mt} Z_t + \omega^2 v_m v_t M_{mt}^3 \right)}{v_t^2 R_m^2 + \omega^2 v_m^2 M_{mt}^2} \end{aligned} \quad (13)$$

Next, set the imaginary part of the formula (13) to zero as follows:

$$0 = \frac{j\omega \left(v_m v_t R_m M_{mt} Z_t + \omega^2 v_m v_t M_{mt}^3 \right)}{\left(v_t R_m \right)^2 + \omega^2 \left(v_m M_{mt} \right)^2} \quad (14)$$

Finally, C_t can be obtained by rearranging equation (14), as in (18):

$$v_m v_t R_m M_{mt} Z_t = -\omega^2 v_m v_t M_{mt}^3 \quad (15)$$

$$Z_t = R_t + j\omega L_t + \frac{1}{j\omega C_t} = \frac{-\omega^2 M_{mt}^2}{R_m} \quad (16)$$

$$\frac{1}{j\omega C_t} = \frac{R_t R_m + j\omega L_t R_m - \omega^2 M_{mt}^2}{R_m} \quad (17)$$

$$C_t = \frac{R_m}{\omega^2 L_t R_m - j\omega \left(R_t R_m + \omega^2 M_{mt}^2 \right)} \quad (18)$$

Based on the derivation of the above formula, the compensation capacitance of the inner and outer coils can be obtained. Further, a resonance characteristic analysis is carried out via simulation according to the resonance compensation capacitance of each resonance tank obtained from the formulas (12) and (15). Since the compensation capacitance makes its impedance resistive, to achieve zero-voltage

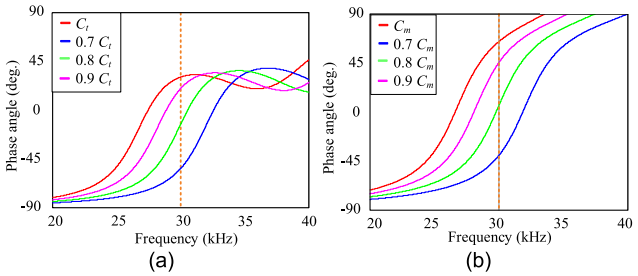

FIGURE 11. Bode diagrams of the resonance phases with different compensation capacitances, (a) impedance phase of the inner heating coil, and (b) impedance phase of the outer heating coil.

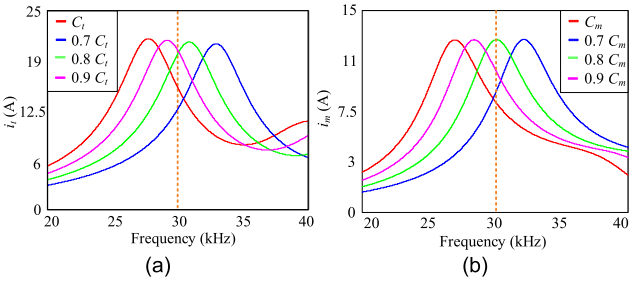

FIGURE 12. Resonance current gains with different resonance compensation capacitance, (a) current in the inner heating coil, and (b) current in the outer heating coil.

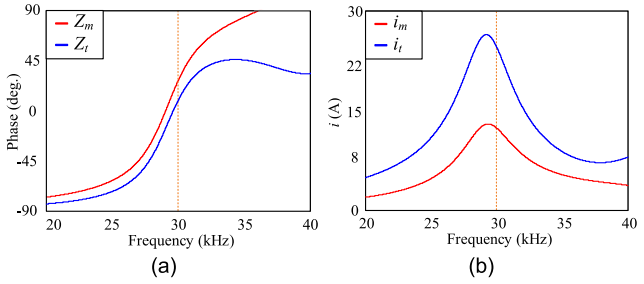

FIGURE 13. Each impedance phase of 0.8 Cm and 0.9 Ct double-loop heating coil and the current flow diagram of each heating coil, (a) impedance phase, and (b) current.

switching (ZVS) and sufficient current gain, its resonant tank characteristics must be adjusted. In this paper, 30 kHz is set as the operating frequency to observe the impact of different resonance compensation capacitances on the impedance phase and current of the resonance tank. Figure 11 shows the resonance impedance phase Bode diagram with different resonance compensation capacitance at 70%, 80%, 90%, and 100% of the preset values C_t and C_m. Figure 11(a) and (b) demonstrate the influence of resonance compensation capacitors on the impedance phase of the resonance tank for the inner heating coil and the outer heating coil, respectively. In Figure 11(a) for the inner heating coil at 30 kHz, when 0.7 C_t and 0.8 C_t are selected, the impedance phases are all below 0 degrees and the input equivalent impedance of the inner coil will appear capacitive. When 0.9 C_t and C_t are selected, the impedance phases are above 0 degrees, and the input equivalent impedance of the inner loop will both be inductive. Observing the impedance phase chart of the outer heating coil in Figure 11(b), when 0.7 C_m is selected, the impedance phase is below 0 degrees, and the input equivalent impedance of the outer coil will appear capacitive. When 0.8 C_m, 0.9 C_m, and C_m are chosen, the impedance phases are all above 0 degrees. As a result, the input equivalent impedance of the outer coil will appear inductive. To make the resonant tank inductive to meet the zero-voltage switching (ZVS) conditions for the power transistors. The configuration of the compensation capacitor of the dual-loop heating coil is set as follows. 0.9 C_t and C_t will be chosen for the inner coil resonance compensation capacitor, while the outer coil resonance compensation capacitance will be set as 0.8 C_m, 0.9 C_m, or C_m.

Next, the resonance tank current corresponding to different resonance compensation capacitances is analyzed, as shown in Figure 12. Figure 12(a) shows the resonant tank currents with different resonance compensation capacitance for the inner heating coil. It can be noted from this figure that although the resonant tank currents at both 0.8 C_t and 0.9 C_t are both high, the phase with 0.8 C_t can be found to be capacitive. While the phase with 0.9 C_t is inductive, the current ramps up to 20 A. Figure 12(b) shows the resonant tank currents with different resonant compensation capacitances for the outer heating coil. The resonant tank current of 0.8 C_m is the highest, with the peak at 12.3 A. Since the input impedance now appears resistive, zero voltage switching (ZVS) can also be achieved.

According to Figure 12, the capacitance yielding higher current is selected and compared with the impedance phase in Figure 11. 0.8 C_m and 0.9 C_t are chosen as the resonance compensation capacitances of the proposed dual-loop heating coil system. Subsequently, focus on the choice of the inner and outer loop compensation capacitors to match each other for analysis. Figure 13 shows the impedance phase and resonant current with 0.8 C_m and 0.9 C_t. First, it can be observed from Figure 13(a) that, with this choice, the impedance phase is greater than 0 degrees at 30 kHz for both input impedance Z_m from the outer loop and the input impedance Z_t from the inner loop. The system is slightly inductive and can achieve zero-voltage switching (ZVS). It can be noted in Figure 13(b) that the outer loop current can reach 11.8 A, while the inner loop current can reach 24.2 A. With 0.8 C_m and 0.9 C_t, both the resultant current and impedance phase meet the requirements set in this paper.

After confirming the resonance compensation capacitance of the inner and outer coil resonant tanks, the impact of this system on each resonant tank under different loads is studied and illustrated in Figure 14. Figure 14(a) shows the influence of different loads on the impedance phase of the inner heating coil. It can be observed that when the operating frequency of the system is 30 kHz, regardless of the load, the equivalent resistance of the inner heating coil has an impedance phase greater than 0 degrees, exhibiting inductive resonance

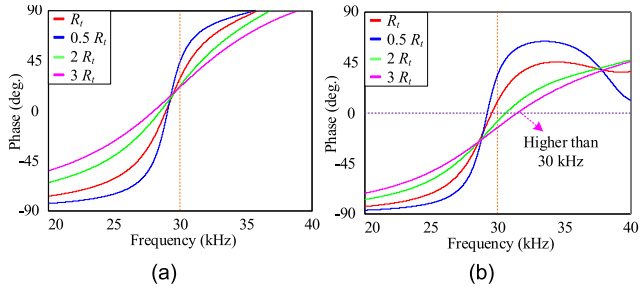

FIGURE 14. The impedance diagrams of dual-loop coil with different loads, (a) input impedance of the inner heating coil and (b) input impedance of the outer heating coil.

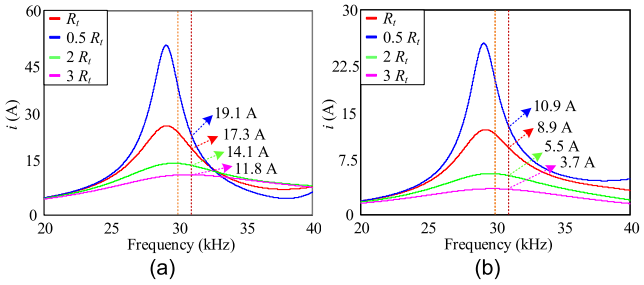

FIGURE 15. The current diagram of different loads in the double-loop coil, (a) current in the inner heating coil, and (b) current in the outer heating coil.

characteristics. This is beneficial for power transistors to achieve zero-voltage switching (ZVS). Figure 14 (b) shows the influence of different loads on the impedance phase of the outer heating coil. When the operating frequency of the system is 30 kHz, the light loads (2 R_t and 3 R_t) render the equivalent impedance phase of the outer heating coil negative, showing slightly capacitive. Therefore, to achieve zero voltage switching (ZVS), its operating frequency will be set at slightly higher than 30 kHz (about 31.5 kHz), to maintain inductive resonant characteristics.

Figure 15(a) and Figure 15(b) show the current variation from different loads in both heating coils. If the operating frequency is 31.5 kHz with 0.8 C_m, 0.9 C_t, and R_t, the outer coil current will be slightly lower than that of 30 kHz but still can reach 17.3 A. The inner coil current is also slightly lower than that of 30 kHz, but will still reach 8.9 A. It can also be found that when the load is heavier, the current in the resonant tank will be higher, and vice versa. The component parameters are listed in Table 2.

V. CONTROL ARCHITECTURE AND ITS UNDERLYING PRINCIPLE

To achieve a stable output voltage to drive the induction heating system, the control system adopts constant voltage and linearly adjusted output power control, by adjusting the control signal of the power transistor for energy delivery. This is to stabilize the constant output of energy in the heating coil. This section will describe the control system in detail, as shown in Figure 16(a). The control system proposed in

TABLE 2. Units for magnetic properties.

Symbol	Description	Value
V_{in}	Input voltage	150 V
$Q_1 \sim Q_5$	Power crystal for compound bridge commutation circuit	IXFH44N50P (500 V / 44 A)
L_m	Resonant inductance of outer heating coil	421.28 μH
L_t	Resonant inductance of inner heating coil	95.53 μH
C_m	Resonant capacitance of the outer heating coil	55.33 nF
C_t	Resonant capacitance of the inner heating coil	224.93 nF
R_m	Equivalent impedance of outer heating coil	18.90 Ω
R_t	Equivalent impedance of inner heating coil	1.94 Ω
M_{mt}	Mutual inductance of dual heating coils	71.50 μH

this paper includes a microcontroller, a driver circuit, and a feedback circuit. When the main power supply provides DC voltage V_{in} and DC current I_{in} to the composite bridge inverter circuit, by adjusting the operating frequency of the power transistors, V_{in} is converted into high-frequency and high-voltage driving voltage v_m and v_t for the dual-loop heating circuit. Moreover, v_m and v_t deliver energy to the heating load. Subsequently, the feedback circuit samples and scales down V_{in} and I_{in} to convert them into DC feedback voltage signal V_{Vin} and current signal V_{Iin} for feeding into the microcontroller. The microcontroller will digitize the signal ($V_{Vin,dig}$ and $V_{Iin,dig}$) and compare them with the voltage and current reference $V_{Vin,ref}$ and $V_{Iin,ref}$ and compute the error voltage value (e_{Vin} and e_{Iin}). After the computation, judgment, and processing by the internal compensator, drive signals are generated by the frequency modulation module at f_{dual}, f_{inner}, and f_{outer}, the corresponding operating frequencies. Moreover, these signals of the corresponding operating frequencies are amplified to v_{gs1}-v_{gs5} by the power transistor driving circuit, and the power transistors are controlled properly by v_{gs1} to v_{gs5}, which can effectively stabilize the power of the heating coil and achieve a good heating effect.

Finally, the control process of the microcontroller will be explained. As shown in Figure 16(b), the proposed bridge-type induction heating system with a flexible switching mechanism can achieve stable heating effects according to the selected power supply mode in this paper. Therefore, the output power will be calculated according to the input voltage and input current, and the operating frequency of the power transistor will be adjusted according to the change. In the initial state of the system, the power supply mode needs to be selected, and the power level P_{ref} and the operating frequency f_s will be set as reference values for power mode selection, to prevent the system from being faulty in the initial state and causing invalid control. After setting the power level P_{ref} and the operating frequency f_s, the system will detect the input feedback V_{in} and I_{in} and calculate the value of the

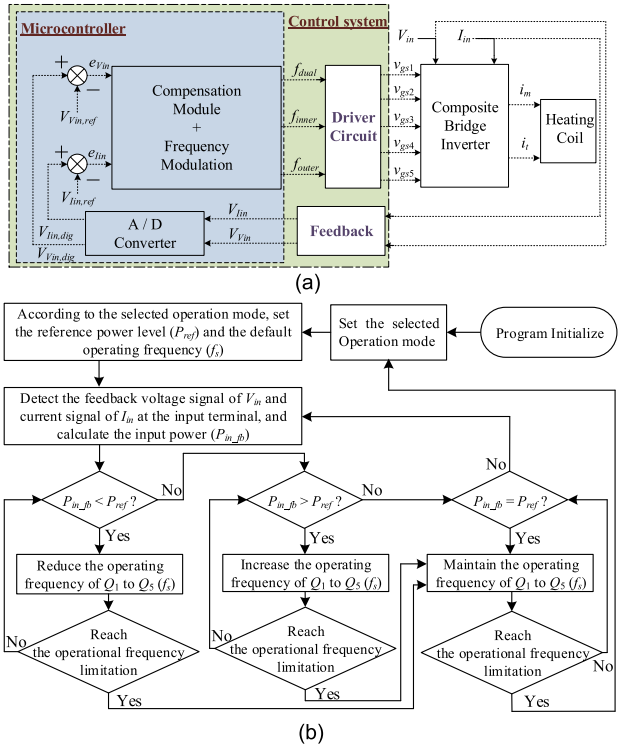

FIGURE 16. Schematic diagram of the control structure of the compound bridge converter circuit system, (a) Control block diagram of induction heating system, and (b) Microcontroller and feedback control flow chart.

current input power P_{in_fb}. Then, P_{in_fb} will be compared with the power level P_{ref}. If the input power P_{in_fb} is lower than the power level P_{ref}, this means that the induction heating effect has not reached the preset goal. As a result, the operating frequency f_s of the power transistors Q_1-Q_5 will be reduced, so that the resonant characteristic of coil-circuit can be changed to be more resistive to increase the input power. When the current input power P_{in_fb} is greater than the power level P_{ref}, it means that the induction heating effect exceeds the preset goal. At this moment, the operating frequency f_s of the power transistors Q_1-Q_5 will be increased to deviate the operating frequency and reduce the input power. If the input power P_{in_fb} is equal to the power level P_{ref}, it means that the induction heating effect meets the desired goal, and the operating frequency f_s of Q_1-Q_5 will be maintained. After comparing P_{in_fb} and P_{ref}, if the power supply mode is updated, the system will update the power reference P_{ref} and the default operating frequency f_s and compare the incoming power P_{in_fb} with the power level P_{ref} to ensure stable input power. If the power supply mode is not updated, the system control will be used to repeatedly detect and calculate P_{in_fb}. Moreover, P_{in_fb} will be continuously compared with power level P_{ref} to ensure the stability of the output power.

VI. EXPERIMENTAL RESULTS

To verify the flexible switching mechanism and the feasibility of the circuit hardware and its control proposed in this paper,

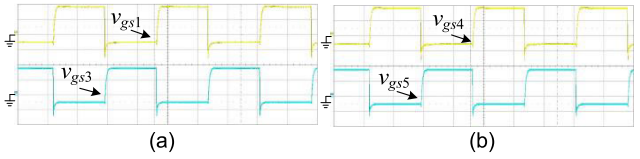

FIGURE 17. Driving signal waveforms of power transistors in dual-loop mode, (a) driving signals of Q_1 and Q_3, and (b) driving signals of Q_4 and Q_5 (v_{gs1}: 10 V/div, v_{gs3}: 10 V/div, v_{gs4}: 10 V/div, v_{gs5}: 10 V/div, Time: 10 μs/div).

a prototype hardware has been built in the laboratory for experiments, and verifications will be discussed in different modes which include dual-loop power supply mode, inner-loop power supply mode, and outer-loop power supply mode. Further, the resonance characteristics, zero voltage switching (ZVS), and the relation between nodal voltage and the duty cycles of the power transistors are analyzed during each mode. Finally, the operating modes changing and heating capability of the proposed composite bridge circuit are verified by these test results, including operations in heating scenarios and temperature distributions on the load.

First, verifications are carried out on the dual-loop power supply mode. In this mode, both coils are in the main heating state, and the power transistors Q_1 and Q_5 are simultaneously both turned on or cut off. The power transistors Q_3 and Q_4 are also turned on or off at the same time. The power transistor Q_2 is always on. The switching of transistors (Q_1 and Q_3) and the switching of transistors (Q_4 and Q_5) are mutually complementary. Figure 17(a) and (b) are driving signal waveform diagrams of power transistors, where the conducting periods of power transistors Q_1 and Q_5 are opposite to those of Q_3 and Q_4. Figure 18 presents the voltage and current waveform diagram of the resonant tank of the inner and outer coils in the dual-loop power supply mode. When the heating system operates in this mode, the phase of the voltage and current in both coils (v_m, i_m, v_t, and i_t) can be observed from this figure. The currents lag the voltages by an angle (θ_m and θ_t), respectively. This also indicates that when the dual-loop power supply is used, both the inner and outer coil resonant tanks are operating inductively, in which condition the zero-voltage switching (ZVS) can be achieved. Figure 19 shows the voltage and current waveform diagrams of the power transistors in the dual-loop power supply mode. From Figure 19(a) and (b), the voltage and current between Q_1 and Q_3 and the relationship between the voltage and current between Q_4 and Q_5 can be observed, the voltage and current waveforms marked with red circles show that the power transistors of the system can indeed achieve zero voltage switching (ZVS) in this mode. The aforementioned waveforms have demonstrated the circuit actions and the status of the power transistors in the dual-loop power supply mode.

The heating effect will be explained in the following. Figure 20 shows the temperature variations in time and heat distribution over the heated load in the dual-loop power

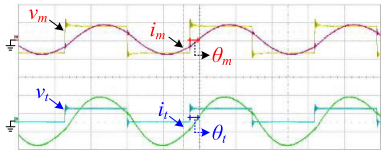

FIGURE 18. Voltage and current waveforms of the inner and outer coil resonance tank in dual-loop mode. (v_m: 200 V/div, i_m: 10 A/div, v_t: 200 V/div, i_t: 10 A/div, Time:10 μs/div).

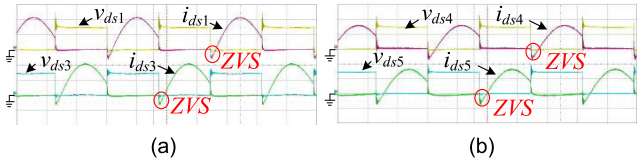

FIGURE 19. Current and Voltage waveforms of power transistors in dual-loop mode, (a) voltage and current of Q_1 and Q_3, and (b) voltage and current of Q_4 and Q_5 (v_{ds1}: 100 V/div, i_{ds1}: 10 A/div, v_{ds3}: 100 V/div, i_{ds3}: 10 A/div, v_{ds4}: 100 V/div, i_{ds4}: 5 A/div, v_{ds5}: 100 V/div, i_{ds5}: 5 A/div, time:10 μs/div).

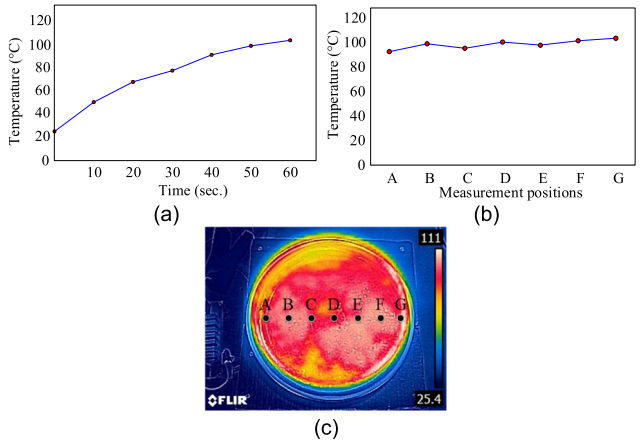

FIGURE 20. Load temperature change and distribution in dual-loop mode, (a) the relationship between temperature and time, (b) temperature distribution status, and (c) thermal imaging measurement photo.

supply mode. Figure 20(a) shows the relationship between temperature and time. Since the system output power is up to 1400 W in this mode, it only takes 60 seconds to heat up to 105.2 degrees Celsius. From Figure 20(b), it can be observed that the heat distribution of the dual-loop power supply mode is quite even, and the average temperature of the 7 spots on the heated load is about 100 degrees Celsius. Figure 20(c) shows a photo taken by the thermal imager which confirms this, for the colors on the photo appear to be very similar, which implies uniform heating. The experiment results in Figure 20 show that this system is capable of fast and uniform heating when working in the dual-loop power supply mode.

In this section, verifications are analyzed for the outer loop power supply mode. In this mode, the outer loop coil is the main heating coil, since mutual inductance and the turning off of power transistors occur, while there is a current passing through the inner coil and generating a magnetic field. The

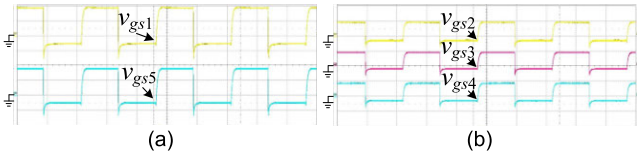

FIGURE 21. Driving signal waveforms of power transistors in outer-loop mode, (a) driving signals of Q_1 and Q_5, and (b) driving signals of Q_2, Q_3, and Q_4. (v_{gs1}: 10 V/div, v_{gs5}: 10 V/div, v_{gs2}: 20 V/div, v_{gs3}: 20 V/div, v_{gs4}:20 V/div, Time:10 μs/div).

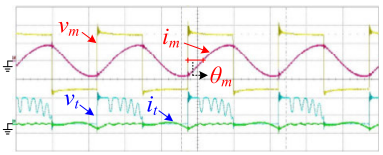

FIGURE 22. Voltage and current waveform diagram of outer ring resonant tank in outer ring power supply mode. (v_m: 100 V/div, i_m: 5 A/div, v_t: 100 V/div, i_t: 5 A/div, time:10 μs/div).

power transistors Q_1 and Q_5 are turned on and off at the same time, while power transistors Q_2, Q_3, and Q_4 are turned on and off at the same time. The switching of transistors (Q_1 and Q_5) and the switching of transistors (Q_2, Q_3, and Q_4) are mutually complementary. Figure 21 is the driving signal waveform diagram of the power transistors, in which the conducting periods of the power transistors Q_1 and Q_5 are the same as shown in Figure 21(a), and the conducting periods of Q_2, Q_3, and Q_4 are also the same as shown in Figure 21(b). Figure 22 is the voltage and current waveform diagram of the resonant tank for the inner and outer coils operating in the outer coil power supply mode. From this figure, it can be found that i_m lags behind v_m by an angle (θ_m), and this presents that the outer loop coil and its compensation capacitor are inductive, which meets the condition of zero voltage switching at this time.

In addition, because the outer coil and its compensation capacitor are receiving the energy provided by the main power supply, the voltage and current waveforms of the resonant circuit (v_m and i_m) are larger than the inner loop (v_t and i_t). Besides, because the inner coil will induce the energy from the outer coil and constitute a conducting loop through other power transistors, the resonant voltage and current in the inner coil remain nonzero. However, because the current of the outer coil power supply is smaller compared with that in dual-loop power supply mode, the induced current in the inner coil part is almost zero. It is noted that because the inner coil is not powered in this mode, a resonance occurred due to the self-inductance or leakage inductance of the inner coil and its compensation or stray capacitance, the resonance voltage of the inner coil exhibits an oscillation before dropping to zero. Since this resonant tank is inductive and meets the zero-voltage switching (ZVS) condition, the zero-voltage switching is verified in the following. Figure 23 shows waveform diagrams of the voltages and currents of the power transistors in the outer loop power supply mode. Figure 23 (a),

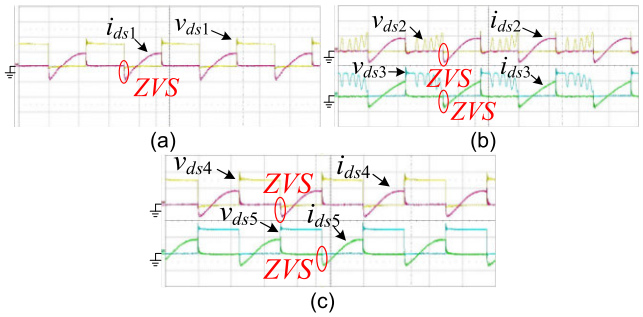

FIGURE 23. Waveform diagram of power crystal voltage and current in outer loop power supply mode, (a) voltage and current of Q_1, (b) voltage and current of Q_2 and Q_3, and (b) voltage and current of Q_4 and Q_5. (v_{ds1}: 100 V/div, i_{ds1}: 5 A/div, v_{ds2}: 100 V/div, i_{ds2}: 5 A/div, v_{ds3}: 100 V/div, i_{ds3}: 5 A/div, v_{ds4}: 100 V/div, i_{ds4}: 5 A/div, v_{ds5}: 100 V/div, i_{ds5}: 5 A/div, time:10 μs/div).

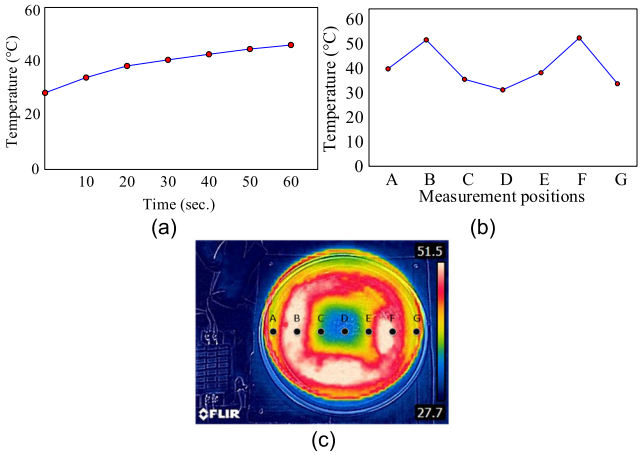

FIGURE 24. Figure of temperature change and its distribution in outer ring power supply mode, (a) the relationship between temperature and time, (b) temperature distribution status, and (c) thermal imaging measurement photo.

(b), and (c) are the voltage and current waveform diagrams of Q_1, Q_2 and Q_3, Q_4 and Q_5 respectively. It can be confirmed from the figure that all power transistors can achieve zero voltage switching (ZVS) in the outer coil power supply mode.

The above evaluates the hardware circuit and its control. Next, the heating effect will be analyzed in the following. Figure 24 shows the load temperature change in time and heat distribution in the outer loop power supply mode. Figure 24(a) shows the temperature of the outer coil over time. It can be observed from the diagram that the temperature can reach 43.6 degrees within 60 seconds. Note that this mode mainly heats the outer coil with a 170 W power supply. Further, in Figure 24(b), it can be observed that the hottest spots are at point B and point F with a temperature of about 51 degrees Celsius. This is confirmed by the actual photo taken by the thermal imager as shown in Figure 24(c), in which the temperature at the outer spots is higher than those located near the center. In this power supply mode, the outer coil can indeed be heated independently, and its local heating effect is apparent. Given the above, the system achieves the desired effect of local heating in the outer loop power supply mode.

Finally, the functions of the inner loop power supply mode are explained in this section. In this mode, the inner coil is powered for heating. Since turning off power transistors and mutual inductance induce a current in the outer coil, it still generates a magnetic field. The power transistors Q_1 and Q_3 are complementary in status. Q_2 is always on. Figure 25(a) presents the driving signal waveform diagram of the power transistors Q_1 and Q_3, where the conducting periods of the power transistors Q_1 and Q_3 are opposite and complementary. The voltage and current waveform diagram of the resonant tank of the inner coil and the outer coil during the inner coil power supply mode is shown in Figure 26(b). Note that the resonant currents in both coils lag the voltages by an angle (θ_t and θ_m), which implies that both coils along with their compensation capacitors appear inductive, which meets the condition of zero voltage switching (ZVS). In addition, because the outer loop coil will induce the energy from the inner loop coil and generate a current through other power transistors and the outer loop current is smaller, the resonant voltage and current still exist in the outer loop. As shown in Figure 25(c), since the inductive resonant circuit achieves zero-voltage switching conditions, the voltage and current waveforms of Q_1 and Q_3 are shown clearly, and ZVS is achieved in Q_1 and Q_3 in the inner loop power supply mode. In the following, the heating effect will be analyzed in the following. Fig. 26 shows the temperature change and heat distribution in the inner loop power supply mode. Figure 26(a) illustrates temperature changes to time. It can be observed from the diagram that the temperature can reach 60 degrees within 60 seconds. Since from Figure 26(b), the system mainly heats the central part and the output power is only 330 W in this mode, it can be observed that the hottest spots during the inner loop power supply mode are at the position of point C and point E with a temperature at about 91 degrees C. In Figure 26(c), the thermal image shows the inner part of the load is hotter than the outer part. Thus, in this power supply mode, the inner coil can be heated independently, and the local heating effect is quite apparent. Given the experimental results, in the inner coil power supply mode, the inner local heating speed and performance of this system are as claimed.

Continuing on, validation is carried out specifically on the efficiency aspect based on the circuit architecture shown in Figure 1(a). R_m and R_t are utilized separately as dummy loads for heating and driving loops, with an input voltage of 150 V. The proposed circuit achieves a maximum efficiency of 96.2%, as depicted in Figure 27. Subsequently, in Dual loop mode operating under light, medium, and heavy loads, the system efficiencies are 95.1%, 95.3%, and 95.8% respectively. In the outer loop power supply mode under the same load conditions, the efficiencies are 95.2%, 95.4%, and 95.9%. Lastly, under the inner loop power supply mode, efficiencies are 95.5%, 95.7%, and 96.2% for light, medium,

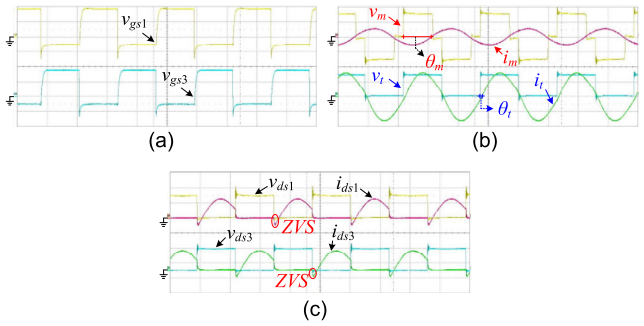

FIGURE 25. Related measurement waveform diagram of power transistors in inner loop power supply mode. (a) driving signals of Q_1 and Q_3, (b) voltage and current waveform diagram of both resonant tanks, and (b) voltage and current of Q_1 and Q_3. (v_{gs1}: 10 V/div, v_{gs3}: 10 V/div, v_m: 100 V/div, i_m: 10 A/div, v_t: 100 V/div, i_t: 10 A/div, v_{ds1}: 100 V/div, i_{ds1}: 10 A/div, v_{ds3}: 100 V/div, i_{ds3}: 10 A/div, time:10 μs/div).

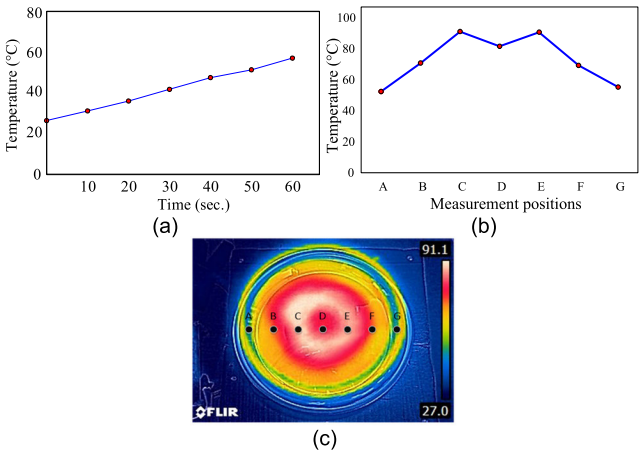

FIGURE 26. Temperature change and heat distribution in the inner loop power supply mode, (a) the relationship between temperature and time, (b) temperature distribution status, and (c) thermal imaging measurement photo.

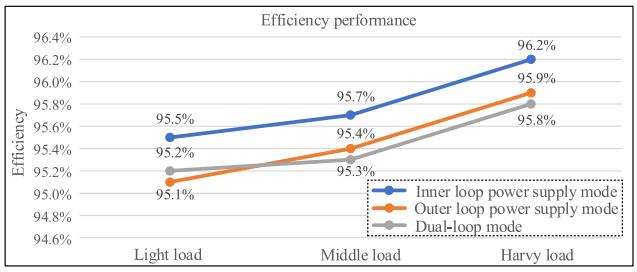

FIGURE 27. Efficiency results in different modes.

and heavy loads. Different operation modes result in varying output powers in light to heavy loads, and the coil and compensation capacitor reach near resonance, most power losses occur in the power transistors. Therefore, in the inner loop power supply mode, higher efficiency is achieved with fewer operational power transistors. In contrast, the other two modes show similar efficiency performances as they have the same number of operating power transistors.

Based on the experimental results, the focus is redirected to the induction heating drive circuit with multiple coils, which is more similar to those in the reference literature. A comparison is made on key aspects such as efficiency, IH load, number of power switches, number of diodes, and power control functions as shown in Table 3. It can be observed from this table that despite having 2 IH loads, the proposed induction heating driving technology in this paper utilizes a coaxial dual-coil with a flexible switching mechanism, which allows each coil to receive simultaneous and independent power transmission, enabling the achievement of three different heating modes for optimizing heating uniformity. Furthermore, compared to the number of power components in other references, the total number of transistors and diodes in the driving circuit proposed in this paper is relatively lower, demonstrating promising efficiency performance.

TABLE 3. Performance comparison of the proposed technology.

Ref.	IH Loads	Transistors	Diodes	Power Control	Eff.
[2]	3	3	0	Conditions	96%
[20]	n	$\sqrt{n}$	$2n$	No	98%
[27]	3	8	0	Conditions	92%
[28]	n	n+1	$2n$	Yes	96%
[29]	2	4+4	0	Conditions	91%
[12]	2	4	0	Yes	97%
Proposed	2*	5	0	Yes	96.2%

*The coil-type is coaxial dual-coil architecture.

Through the above discussion of the system hardware circuit, the control mechanism, and the heating effect in different power supply modes, it can be noted that under the dual-loop power supply mode, due to the supply power being larger, the heating is faster and more uniform. Whereas in the other loop power supply modes, the energy delivered will be smaller, the main reason for such a design is that when the dual-loop power supply mode is adopted and the load has been heated to a certain temperature, depending on the need of the heating task, only the outer coil or inner coil will be locally heated. When there is only one loop turned on in this system, due to mutual inductance, energy will also be induced in the unpowered coil, and it forms a current loop through its power transistors and generates magnetic energy to supply the load for heating. Therefore, even for local heating needs, other parts of the load can still receive some heat, which is beneficial to the overall heating speed. Through the temperature measurement over time, temperature measurements at multiple spots and thermal imager photos, it is demonstrated that the heating speed and performance of the proposed induction heating system have achieved the expected results in three power supply modes. It also proves the effectiveness of the proposed composite bridge-type circuit, which is capable of flexibly switching and driving the dual-loop coil structure. In contrast with the results from earlier studies in which each coil must have an exclusive driving circuit, this design greatly enhances the overall competitiveness.

VII. CONCLUSION

This paper realizes a design of the composite bridge-type inverter with a flexible switching mechanism for a coaxial dual-coil induction heating system, which can indeed enhance the heating effect. With a single inverter circuit,

it can drive either or both sets of coils, and designate the specific coil to heat, which greatly improves the application flexibility. The proposed dual-coil power supply mode mechanism, combined with the composite inverter design, adjusts the operating frequency of power transistors to change the resonant input voltage and current, thereby eliminating the uneven heating of the load. In addition to the dual-loop power supply mode, the hybrid switching design of the composite inverter circuit can switch the system to operate in the outer loop power supply mode or the inner loop power supply mode to perform the heating task for a specific area of the load. Through careful analysis of circuit principles, detailed explanation of control mechanisms, and practical tests of various power supply modes of hardware circuits, it can be found that the composite bridge-type rectifier circuit proposed in this article can achieve fast heating, local heating, and uniform heating effects under various power supply modes, truly achieving high flexibility in driving dual-coil structures. These test results will be beneficial for the design reference and application value of the related industries of induction heating systems, and contribute to the improvement of industrial and everyday applications.

REFERENCES

[1] O. Lucia, D. Navarro, P. Guillén, H. Sarnago, and S. Lucia, "Deep learning-based magnetic coupling detection for advanced induction heating appliances," *IEEE Access*, vol. 7, pp. 181668–181677, 2019.

[2] B. Salvi, S. Porpandiselvi, and N. Vishwanathan, "A three switch resonant inverter for multiple load induction heating applications," *IEEE Trans. Power Electron.*, vol. 37, no. 10, pp. 12108–12117, Oct. 2022.

[3] J. Choi, T. Kim, C.-K. Lee, and S.-K. Kim, "Design and performance analysis results of iron-core type MgB_2 and HTS magnets for large-scale superconducting induction heaters," *IEEE Trans. Appl. Supercond.*, vol. 30, no. 4, pp. 1–4, Jun. 2020.

[4] C.-J. Chang, C.-C. Tai, F.-W. Lin, C.-C. Kuo, and C.-M. Hung, "Effects of flexible induction coil pitch on the heating performance of thermotherapy needles," *IEEE Trans. Instrum. Meas.*, vol. 69, no. 11, pp. 8983–8991, Nov. 2020.

[5] M. Pérez-Tarragona, H. Sarnago, Ó. Lucía, and J. M. Burdío, "Multiphase PFC rectifier and modulation strategies for domestic induction heating applications," *IEEE Trans. Ind. Electron.*, vol. 68, no. 8, pp. 6424–6433, Aug. 2021.

[6] J. Serrano, I. Lope, and J. Acero, "Nonplanar overlapped inductors applied to domestic induction heating appliances," *IEEE Trans. Ind. Electron.*, vol. 66, no. 9, pp. 6916–6924, Sep. 2019.

[7] S. Eom, H. Zhou, U. Kaur, R. M. Voyles, and D. Kusuma, "TupperwareEarth: Bringing intelligent user assistance to the 'Internet of Kitchen Things,'" *IEEE Internet of Things J.*, vol. 9, no. 15, pp. 13233–13249, Aug. 2022.

[8] R. Sagues-Tanco, L. Benages-Pardo, G. López-Nicolás, and S. Llorente, "Fast synthetic dataset for kitchen object segmentation in deep learning," *IEEE Access*, vol. 8, pp. 220496–220506, 2020.

[9] M.-S. Huang, C.-C. Liao, Z.-F. Li, Z.-R. Shih, and H.-W. Hsueh, "Quantitative design and implementation of an induction cooker for a copper pan," *IEEE Access*, vol. 9, pp. 5105–5118, 2021.

[10] J. Acero, C. Carretero, R. Alonso, and J. M. Burdio, "Quantitative evaluation of induction efficiency in domestic induction heating applications," *IEEE Trans. Magn.*, vol. 49, no. 4, pp. 1382–1389, Apr. 2013.

[11] O. Lucía, P. Maussion, E. J. Dede, and J. M. Burdío, "Induction heating technology and its applications: Past developments, current technology, and future challenges," *IEEE Trans. Ind. Electron.*, vol. 61, no. 5, pp. 2509–2520, May 2014.

[12] H. Sarnago, Ó. Lucía, M. Pérez-Tarragona, and J. M. Burdío, "Dual-output boost resonant full-bridge topology and its modulation strategies for high-performance induction heating applications," *IEEE Trans. Ind. Electron.*, vol. 63, no. 6, pp. 3554–3561, Jun. 2016.

[13] J. Serrano, J. Acero, I. Lope, C. Carretero, and J. M. Burdío, "A flexible cooking zone composed of partially overlapped inductors," *IEEE Trans. Ind. Electron.*, vol. 65, no. 10, pp. 7762–7771, Oct. 2018.

[14] S. H. Im, J. S. Kim, Y. S. Jang, and G. S. Park, "Design of ferrite core for the improvement of power efficiency in induction range," *IEEE Trans. Magn.*, vol. 55, no. 6, pp. 1–4, Jun. 2019.

[15] H. Sarnago, O. Lucía, and J. M. Burdio, "A versatile resonant tank identification methodology for induction heating systems," *IEEE Trans. Power Electron.*, vol. 33, no. 3, pp. 1897–1901, Mar. 2018.

[16] Ó. Lucia, C. Carretero, J. M. Burdio, J. Acero, and F. Almazan, "Multiple-Output resonant matrix converter for multiple induction heaters," *IEEE Trans. Ind. Appl.*, vol. 48, no. 4, pp. 1387–1396, Jul. 2012.

[17] C. Carretero, O. Lucia, J. Acero, and J. M. Burdio, "Computational modeling of two partly coupled coils supplied by a double half-bridge resonant inverter for induction heating appliances," *IEEE Trans. Ind. Electron.*, vol. 60, no. 8, pp. 3092–3105, Aug. 2013.

[18] W. Han, K. T. Chau, and Z. Zhang, "Flexible induction heating using magnetic resonant coupling," *IEEE Trans. Ind. Electron.*, vol. 64, no. 3, pp. 1982–1992, Mar. 2017.

[19] M. Aoyama, W. Thimm, M. Knoch, and L. Ose, "Proposal and challenge of Halbach array type induction coil for cooktop applications," *IEEE Open J. Ind. Appl.*, vol. 2, pp. 168–177, 2021.

[20] H. Sarnago, P. Guillén, J. M. Burdío, and O. Lucia, "Multiple-output ZVS resonant inverter architecture for flexible induction heating appliances," *IEEE Access*, vol. 7, pp. 157046–157056, 2019.

[21] E. Plumed, I. Lope, and J. Acero, "Induction heating adaptation of a different-sized load with matching secondary inductor to achieve uniform heating and enhance vertical displacement," *IEEE Trans. Power Electron.*, vol. 36, no. 6, pp. 6929–6942, Jun. 2021.

[22] R. C. M. Gomes, M. A. Vitorino, D. A. Acevedo-Bueno, and M. B. de R. Corrêa, "Three-phase AC–AC converter with diode rectifier for induction heating application with improved input current quality and coil modeling," *IEEE Trans. Ind. Appl.*, vol. 57, no. 3, pp. 2673–2681, May 2021.

[23] W. Han, K. T. Chau, C. Jiang, and W. Liu, "All-metal domestic induction heating using single-frequency double-layer coils," *IEEE Trans. Magn.*, vol. 54, no. 11, pp. 1–5, Nov. 2018.

[24] H. Sarnago, Ó. Lucía, A. Mediano, and J. M. Burdío, "Multi-MOSFET-based series resonant inverter for improved efficiency and power density induction heating applications," *IEEE Trans. Power Electron.*, vol. 29, no. 8, pp. 4301–4312, Aug. 2014.

[25] Y. Hu, B. Ji, S. Finney, W. Xiao, and W. Cao, "High-frequency inverter topologies integrated with the coupled inductor bridge arm," *IET Power Electron.*, vol. 9, no. 6, pp. 1144–1152, May 2016.

[26] S. Porpandiselvi and N. Vishwanathan, "Three-leg inverter configuration for simultaneous dual-frequency induction hardening with independent control," *IET Power Electron.*, vol. 8, no. 9, pp. 1571–1582, Sep. 2015.

[27] S. Khatroth and P. Shunmugam, "Cascaded full-bridge resonant inverter configuration for different material vessel induction cooking," *IET Power Electron.*, vol. 13, no. 19, pp. 4428–4438, Dec. 2020.

[28] P. Guillen, H. Sarnago, O. Lucia, and J. M. Burdio, "GaN-based matrix resonant power converter for domestic induction heating," *IEEE Trans. Power Electron.*, vol. 38, no. 6, pp. 6769–6773, Jun. 2023.

[29] S. K. Papani, V. Neti, and B. K. Murthy, "Dual frequency inverter configuration for multiple-load induction cooking application," *IET Power Electron.*, vol. 8, no. 4, pp. 591–601, Apr. 2015.

TE-CHUN HUNG (Member, IEEE) received the Ph.D. degree in electrical engineering from National Cheng Kung University, Tainan, Taiwan, in 2016.

From 2013 to 2018, he was with Delta Electronics, Inc., Tainan. Since 2018, he has been with the Department of Electrical Engineering, Southern Taiwan University of Science and Technology, Tainan, where he is currently an Associate Professor. His research interests include power electronics circuit design and power electronics applications.

KUAN-CHIEH HUANG (Member, IEEE) was born in Taipei, Taiwan, in 1987. He received the M.S. degree from the Department of Greenergy, National University of Tainan, Tainan, Taiwan, in 2011, and the Ph.D. degree in electrical engineering from National Cheng Kung University, Tainan, in 2018. Since 2021, he has been with the Department of Electrical Engineering, Southern Taiwan University of Science and Technology, as an Assistant Professor, where he teaches and conducts research on power electronics, green energy, and digital signal processing.

TSONG-SHING LEE (Member, IEEE) received the Ph.D. degree in electrical engineering from National Cheng Kung University, Tainan, Taiwan, in 2015. He was with AU Optronics Corporation, Hsinchu, Taiwan, from 2004 to 2016. Since 2016, he has been with the Department of Electrical Engineering, Southern Taiwan University of Science and Technology, Tainan, where he is currently a Professor. His research interests include power electronic converters, inductively coupled power transfer systems, display power supply, resonant circuit, and piezoelectric transformer power application.

JING-HONG LIN was born in Chiayi, Taiwan, in 2000. He received the Bachelor of Science degree in electrical engineering from Southern Taiwan University of Science and Technology, Tainan, Taiwan, in 2023. He is currently pursuing the master's degree with the National Changhua University of Education. His research interests include power electronics, battery equalizers, and energy conversion applications.

CHEIEN-HUA CHEN was born in Chiayi, Taiwan, in 2000. He received the Bachelor of Science degree in electrical engineering from Southern Taiwan University of Science and Technology, Taiwan, Taiwan, in 2023. He is currently pursuing the master's degree with the National Yunlin University of Science and Technology. His research interests include power electronics and high-efficiency DC power converter.

CHI-WEI LIAO was born in Yunlin, Taiwan, in 2000. He received the Bachelor of Science degree in electrical engineering from Southern Taiwan University of Science and Technology, Tainan, Taiwan, in 2023. He is currently pursuing the master's degree with the National Yunlin University of Science and Technology. His research interests include power electronics, power quality, and induction generator applications.